

Cost and Routing of Continuous Variable Quantum Networks

Federico Centrone,^{1,2,*} Frederic Grosshans,^{1,†} and Valentina Parigi^{3,‡}

¹*Sorbonne Université, CNRS, LIP6, 4 place Jussieu, F-75005 Paris, France*

²*Université de Paris, CNRS, IRIF, 8 Place Aurélie Nemours, 75013 Paris, France*

³*Laboratoire Kastler Brossel, Sorbonne Université, CNRS, ENS-Université PSL, Collège de France, 4 place Jussieu, F-75252 Paris, France*

We study continuous-variable graph states with regular and complex network shapes and we report for their cost as a global measure of squeezing and number of squeezed modes that are necessary to build the network. We provide an analytical formula to compute the experimental resources required to implement the graph states and we use it to show that the scaling of the squeezing cost with the size of the network strictly depends on its topology. We show that homodyne measurements along parallel paths between two nodes allow to increase the final entanglement in these nodes and we use this effect to boost the efficiency of an entanglement routing protocol. The devised routing protocol is particularly efficient in running-time for complex sparse networks.

I. INTRODUCTION

Quantum networks theory, i.e. the study of networks of systems with quantum properties, have applications ranging from fundamental research to real-world applications. Many physical systems, such as solid state materials and large molecules like proteins can indeed be modeled as quantum networks. The underlying structure of some quantum systems can deeply influence their properties and the theoretical study of quantum networks can help the understanding of many important phenomena. Photonics quantum networks, for instance, are essential resources for quantum information processing and notably for quantum internet applications, where quantum states of light will allow for the efficient distribution and manipulation of information [1–3]. Needless to say, in order to develop large scale quantum communications and build a quantum internet it is compulsory to grasp the potentialities of quantum networks and exploit all their exceptional features.

There are several ways to supply quantum communication channels among devices placed at different locations, including simple optical fibers and entangled photons. An appealing approach to study photonic quantum networks is given by continuous variables (CV) graph states, an interesting class of Gaussian quantum states that, under certain condition, can provide a substrate for universal quantum computation [4]. This type of quantum states can readily be produced in some well equipped photonic labs, however their ideal version requires an infinite amount of squeezing, which is unphysical as it would imply infinite energy.

In this work we present new methods and results to study CV graph states with regular and complex topologies. CV describes quantum states living in infinite dimensional Hilbert spaces and it is the most natural language for bosonic fields, such as photons. Moreover, generation and measurement of CV states requires only coherent control on classical laser source and weakly non-linear ma-

terials, along with coherent (homodyne) detection which, differently from photon counting detectors, can be highly efficient at room temperature and easily integrated in classical communication networks. However, CV encoding in quantum networking/routing protocols has not been extensively studied yet, unlike the discrete variables (DV) case [5–7].

Our model aims at reproducing the existing photonic platforms with realistic experimental constraints, such as limited amount of squeezing, but without taking into account propagation losses. This work is focused on the capabilities of pure CV quantum states to act as quantum networks and the resources needed for their generation. Generation losses can be very low, so that the hypothesis of pure states is a realistic one, whereas propagation losses can be mitigated by considering local (short distances) networks, and their effect on long distances will be included in future works. At the same time we probe the capabilities of photonic platforms while the scaling of the network increases beyond the capacities allowed by the state-of-the-art technology. Since the main limitation to build these optical systems is finite squeezing, we provide in section III an analytical formula that allows to compute the amount of squeezing in each mode as a function of the spectrum of the underlying graph. We show the graph states' cost as a global measure of squeezing and number of squeezed modes that are necessary to build the network. In particular we explore the cost of different networks topologies in term of number of needed squeezers at fixed number of nodes in the networks and of the global amount of squeezing.

We then explore their potentialities to perform efficient quantum communications between two arbitrary nodes when assisted with a given class of Gaussian Local Operations and Classical Communication (GLOCC) by all the agents in the network. A typical approach of quantum networking and routing consists in distributing photonics states like single-photons, Bell pairs or Gaussian states and then use synchronous local operations that build the wanted entanglement structure between the agents [2, 8–14]. We rather consider the case where a preexisting CV multipartite entangled state is distributed among the players and then local operations reconfigure the entanglement connections, similarly to some protocol in the DV case [15]. The choice is motivated by the fact that multimode entangled states can be directly gener-

*Currently at ICFO-Institut de Ciències Fòtiques, Castelldefels (Barcelona), Spain; Electronic address: federico.centrone@icfo.eu

†Electronic address: frederic.grosshans@lip6.fr

‡Electronic address: valentina.parigi@lkb.upmc.fr

ated via optical platform [16–20] and their shape can be easily manipulated [21, 22]. We show, both analytically and numerically that in specific topologies homodyne measurements along parallel paths allow to increase the entanglement between two distant nodes.

Finally, we devise a routing protocol based on local quadrature measurements for reshaping the network in order to perform a teleportation protocol between two arbitrary nodes of the networks. The *Routing* protocol, which is based on wire-shortening over parallel paths among the nodes, improves the final entanglement between the two nodes in a considerable amount of cases, and it is particularly efficient in running-time for complex sparse networks.

The article is structured as it follows. In section II we discuss Gaussian quantum states, their generation by quadratic Hamiltonian and their decomposition. We then introduce the Gaussian quantum networks studied in this Article. In section III, we derive the first result of this paper, namely an equation providing the squeezing values required to experimentally build a graph state as a function of its graph spectrum. In section IV we revise a resource theory of squeezing and in section V we will adopt it in order to estimate the cost of expanding the network. Although in entangled qubits networks the resource usage is always proportional to the number of links, we show that in CV Gaussian networks the trend of the presents non-trivial scaling with the size of the network and this is strictly dependent on its topology. We present as well a few instances of the full squeezing spectra — i.e. the needed amount of squeezers with the required squeezing values — of regular and complex networks, showing that some topologies are equivalent up to a linear optical transformation.

In section VI we propose a CV architecture for the quantum internet based on the Gaussian network previously described. We simulate quantum communication protocols through the network by letting the spatially separated agents present at each node perform a homodyne measurement on their optical mode and look for the optimal measurement strategy to maximize the negativity of the entangled pair shared by the two users who want to communicate, Alice and Bob. We prove that when multiple entangled paths connect Alice to Bob the optimal measurement strategy allows to increase the negativity in the final pair. This *parallel enhancement of entanglement* can be used to increase the quality of quantum communications in some selected network topologies.

Lastly, in section VIII, we employ our previous findings to implement an heuristic routing protocol for distributing and boosting the entanglement between two arbitrary agents. The algorithm we provide, on the one hand, is much more efficient than directly checking all possible combinations of quadrature measurements and, on the other hand, it always provides higher negativity than the classical scheme, which is directly employing the shortest path between Alice and Bob and neglect the parallel channels.

II. ARBITRARY GAUSSIAN NETWORK

A. Gaussian quantum states

The generation of continuous variables multimode entangled states has been demonstrated in several optical setups. In such experiments we recover networks structures as naturally appearing entanglement correlations [18], reconfigurable Gaussian interactions [22], or imprinted cluster states [16, 17, 20, 21, 23].

These quantum states produced via parametric processes and linear optical transformations are characterized by Gaussian statistical distribution of the quadratures of the involved optical modes [24]. The quadratures \hat{q}_j and \hat{p}_j of the j^{th} mode are canonical conjugate variables, such that $[\hat{q}_j, \hat{p}_k] = i\delta_{j,k}$, associated to the quantum harmonic oscillator describing the light mode. In this work we adopt the following relation with creation and annihilation operators $\hat{\mathbf{a}}^\dagger = (\hat{\mathbf{q}} - i\hat{\mathbf{p}})/\sqrt{2}$ and $\hat{\mathbf{a}} = (\hat{\mathbf{q}} + i\hat{\mathbf{p}})/\sqrt{2}$, such that the variance of the vacuum quadratures is normalized to $1/2$.

The produced states can then be completely characterized by the first two moments of the quadratures $\bar{\mathbf{r}} = \text{Tr}[\rho\hat{\mathbf{r}}]$ and $\sigma = \text{Tr}[\rho\{(\hat{\mathbf{r}} - \bar{\mathbf{r}}), (\hat{\mathbf{r}} - \bar{\mathbf{r}})^T\}]$, where ρ is the density matrix of the Gaussian state and $\hat{\mathbf{r}} = (\hat{q}_1 \dots \hat{q}_N, \hat{p}_1 \dots \hat{p}_N)$ — we follow here qp -ordering.

Parametric processes are described by quadratic Hamiltonians $\hat{\mathcal{H}}_I = \hat{\mathbf{r}}H\hat{\mathbf{r}}^T$, whose dynamics is implemented on the quadratures by $S_H = e^{\Omega\hat{H}t}$, as

$$\hat{\mathbf{r}}' = S_H\hat{\mathbf{r}}_0 \quad (1)$$

where $\hat{\mathbf{r}}_0$ are quadratures of the initial state, $\hat{\mathbf{r}}'$ are the quadratures of the final state and $\Omega = \begin{pmatrix} 0 & \mathbb{1} \\ -\mathbb{1} & 0 \end{pmatrix}$ is a $2N \times 2N$ skew-symmetric matrix associated to the N dimensional Hilbert space allowing to write the commutation relation of the canonical variables as

$$[\hat{\mathbf{r}}, \hat{\mathbf{r}}^T] = i\Omega = i \begin{pmatrix} 0 & \mathbb{1} \\ -\mathbb{1} & 0 \end{pmatrix}.$$

Since any pure Gaussian state can be obtained by the application of a unitary generated by a quadratic Hamiltonian H to the vacuum, the most general pure Gaussian state covariance matrix is given by applying S_H by congruence to the vacuum covariance matrix $\sigma_0 = 1/2$:

$$\sigma = S_H\sigma_0S_H^T = \frac{S_HS_H^T}{2} \quad (2)$$

Singular value decomposition allows one to write the symplectic transformation in the so called Bloch-Messiah decomposition [24] as a product of an orthogonal, a diagonal and an orthogonal matrices $S_H = O\Delta O'$, which can be interpreted as a basis rotation, a squeezing in the diagonal basis and another rotation. The mode-basis in which the covariance matrix is diagonal and each component is independently squeezed is named the supermode basis. In [18, 21] where the pump and the phase matching function can be described by a Gaussian spectral profile, the supermode basis corresponds to Hermite-Gauss spectral modes. The squeezing values of Δ can be derived from the eigenvalues of the Hamiltonian $\hat{\mathcal{H}}_I$, while the orthogonal matrix O can be interpreted as a measurement basis

change or, equivalently, as a passive linear optical transformation. The other orthogonal matrix O' is simplified in the product $S_H S_H^T$ and can be disregarded:

$$\sigma = \frac{S_H S_H^T}{2} = \frac{1}{2} O \Delta^2 O^T. \quad (3)$$

The diagonal matrix Δ contains the information on the minimum number of squeezed modes in the system and their value of squeezing, which will later be used in the chosen resource theory. If we consider a single mode field, the squeezing operation is defined as a Gaussian transformation that reduces the variance of \hat{p} by a factor $10^{-s/10}$, where s , measured in dB throughout this article, is called *squeezing factor*. Squeezing is represented by the local symplectic matrix

$$S_{sq}(s) = \begin{pmatrix} 10^{s/20} & 0 \\ 0 & 10^{-s/20} \end{pmatrix}.$$

The multimode Δ matrix can then be written as

$$\Delta = \text{diag}\{10^{s_1/20}, 10^{s_2/20}, \dots, 10^{s_N/20}, 10^{-s_1/20}, 10^{-s_2/20}, \dots, 10^{-s_N/20}\}. \quad (4)$$

This formalism can be used to visualize and manipulate Gaussian quantum states, that are readily available in most well-equipped photonics laboratories and, although the number of modes and their connections is still in large part limited, many efforts are employed to improve the capacities of these systems.

Targeted Gaussian quantum states, including the quantum networks of the next section, can be generated via the two following strategies: i) by tailoring Hamiltonians $\hat{\mathcal{H}}_I$ of multimode parametric processes in order to get the decomposition of eq. (3) corresponding to the desired covariance matrix [19, 21, 25–28]; ii) by getting a number of single-mode squeezers equal to the the number of elements with $s_j \neq 0$ of Δ in eq. (3) and producing the corresponding s_j squeezed states, that are injected in a linear optic interferometer corresponding to the orthogonal matrix O in eq. (3) [29–31].

B. Graph states as quantum networks

The above formalism can be employed to describe Gaussian graph states, that can be used as CV quantum networks. We at first recall that a network is mathematically described by a graph $\mathcal{G}(V, E)$, which is a set of vertices V (or nodes) connected by a set of edges E . Labeling the nodes of the graph in some arbitrary order, we can define a symmetric adjacency matrix $A = A^T$ whose $(j, k)^{\text{th}}$ entry A_{jk} is equal to the weight of the edge linking node j to node k (with no edge corresponding to a weight of 0). Typically, the adjacency matrix is enough to completely characterize a graph, however we will see that in our case there are other degrees of freedom such as the squeezing of a node and its angle.

We can now describe the quantum networks we use in this work that are called graph- or cluster-states ¹

[32–34]. Theoretically, they can be built by entangling a number of squeezed modes of light via CZ-gates, which is a Gaussian operation implementing a correlation of strength g between the \hat{q} and the \hat{p} of the two modes on which it acts. The corresponding symplectic matrix is

$$S_{CZ}(g) = \begin{pmatrix} 1 & 0 & 0 & 0 \\ 0 & 1 & 0 & 0 \\ 0 & g & 1 & 0 \\ g & 0 & 0 & 1 \end{pmatrix}$$

The graph associated to the graph states identify edges as CZ-gates applied between nodes, that are the squeezed modes, weighted with g .

In order to simplify the many degrees of freedom present in our networks, for the moment we shall assume that all the nodes will be squeezed in \hat{p} by s and all the edges have a correlation strength of g . If we apply a CZ-gate network with adjacency matrix A to a multimode squeezed vacuum σ_s , with squeezing factor s we obtain a Gaussian network with covariance matrix [35]

$$\begin{aligned} \sigma &= \begin{pmatrix} \sigma_{qq} & \sigma_{qp} \\ \sigma_{pq} & \sigma_{pp} \end{pmatrix} = \begin{pmatrix} \mathbb{1} & 0 \\ A & \mathbb{1} \end{pmatrix} \sigma_s \begin{pmatrix} \mathbb{1} & A \\ 0 & \mathbb{1} \end{pmatrix} \\ &= \begin{pmatrix} R\mathbb{1} & RA \\ RA & RA^2 + \mathbb{1}/R \end{pmatrix} \end{aligned} \quad (5)$$

Where $R = 10^{s/10}$. The $2N \times 2N$ covariance matrix σ is divided in four $N \times N$ blocks, where the blocks σ_{qq} and σ_{pp} represent the correlations among the different nodes' q - and p -quadratures, respectively, whereas the blocks σ_{qp} and σ_{pq} describes the correlations between q - and p -quadratures.

Bear in mind that the CZ-gate operations that theoretically identify the edges of the networks are seldom realized in any laboratory being very challenging to accomplish. What is commonly done, as explained in the previous subsection, is the reduction of the covariance matrix of the graph state in (5) to the form of eq. (3), that is also a receipt for building the graph states from a certain number of squeezed modes (Δ) and linear optics transformations (O).

III. INTERPLAY BETWEEN SQUEEZING AND ADJACENCY SPECTRA

Consider a N -dimensional graph with adjacency matrix A . If we apply a set of CZ-gates to the set of N modes of a vacuum state according following the edges defined by A , we end up with a Gaussian graph state with the following $2N$ -dimensional covariance matrix:

$$\sigma = \frac{1}{2} \begin{pmatrix} \mathbb{1} & A \\ A & \mathbb{1} + A^2 \end{pmatrix}, \quad (6)$$

where we assumed that the vacuum state variance is normalized to 1/2. Since A is symmetric, it is always

¹ While usually the name cluster is used when the graph shape

allows for universal quantum computing, in this work we will use the terms cluster state and graph state as synonyms.

diagonalizable

$$VAV^T = D = \text{diag}(\{D_i\}), \quad (7)$$

for some orthogonal matrix V , where $\{D_i\}_{i=1}^N$ is the set of the real eigenvalues of A . It follows that $VA^2V^T = VAV^TVAV^T = D^2$. Let us consider the following matrix

$$W = \frac{1}{\sqrt{2}} \begin{pmatrix} V & V \\ V & -V \end{pmatrix}. \quad (8)$$

We can verify easily that $WW^T = \mathbb{1}$, hence W is an orthogonal matrix implementing a basis change that would not change the spectrum of the matrix to which it is applied. If we apply it to σ we get

$$\sigma' = W\sigma W^T = \frac{1}{2} \begin{pmatrix} \mathbb{1} + D + D^2/2 & -D^2/4 \\ -D^2/4 & \mathbb{1} - D + D^2/2 \end{pmatrix}, \quad (9)$$

which is a block matrix composed of diagonal matrices. We can permute the rows and columns of the matrix to get a diagonal block matrix

$$\Pi\sigma'\Pi^T = \bigoplus_{i=1}^N M_i, \quad (10)$$

where Π is a permutation operator, while

$$M_i = \frac{1}{2} \begin{pmatrix} \mathbb{1} + D_i + D_i^2/2 & -D_i^2/4 \\ -D_i^2/4 & \mathbb{1} - D_i + D_i^2/2 \end{pmatrix}. \quad (11)$$

In this basis, each block M_i represents a single mode covariance matrix of a pure unentangled Gaussian state. We can hence diagonalize each block independently. In particular, notice that $\det(M_i) = \frac{1}{4}$, thus the eigenvalues of σ are given by

$$\begin{aligned} \lambda_i^\pm &= \left(\text{Tr}(M_i) \pm \sqrt{\text{Tr}(M_i)^2 - 4\det(M_i)} \right) = \\ &= \frac{1}{2} \left(1 + D_i^2/2 \pm \sqrt{D_i^2 + D_i^4/4} \right). \end{aligned} \quad (12)$$

These values represent the squeezed and antisqueezed variances of the uncoupled oscillators of equation (4), e.g. the uncertainty of measuring the real and imaginary part of the electromagnetic field. Equation (12) shows the interplay between the physical resources necessary to experimentally implement a CV graph state and the spectrum of the underlying graph. This implies that we can use spectral graph theory to characterize analytically the physical requirements of building Gaussian networks and thus predict which one will be easier to realize. A first crucial consequence is that different graph states whose underlying graphs are co-spectral, e.g. their adjacency matrices have the same eigenvalues, can be transformed into each other applying passive linear optics². We will see later in Sec. V A that the star and diamond

networks have this property, making them a relevant class of Gaussian networks for applications. The intrinsic connection between the squeezing of a Gaussian network and its topology was already put in evidence by Gu et al. [34], by proving a relation between the squeezing required to produce a CV graph state and the singular value decomposition of the associated adjacency matrix. Our result is an exact generalization of theorems 2 and 3 of Ref. [34], beyond the limit of large squeezing, i.e. in a regime that is accessible with current technology.

Another crucial consequence of equation (12) is that for CV graph states the number of independent squeezed modes (squeezers) in their Bloch–Messiah decomposition corresponds to the rank $\text{rk}(A)$ of the associated adjacency matrix.

For any non-trivial graph, we have

$$2 \leq \text{rk}(A) \leq N. \quad (13)$$

The impossibility of rank 1 adjacency matrices comes from their null trace. If A is not full-rank, it has a non-null kernel. A common source of such kernels vectors is when one has k linearly sets S_1, \dots, S_k of vertices sharing the same neighborhood AS_1 , where, by a slight abuse of notation, S_i denotes both a set of vertices and the corresponding column vector:

$$\forall 1 \leq i \leq k, \quad AS_i = AS_1. \quad (14)$$

We have then

$$A \sum_{i=1}^k \alpha_i S_i = \left(\sum_{i=1}^k \alpha_i \right) AS_1 \quad (15)$$

Which is null iff $\sum_i \alpha_i = 0$. This gives us a null-eigenspace of dimension $k - 1$.

The most obvious example of this is the star graph, where $N - 1$ vertices share the same neighbor, giving a null space of dimension $N - 1 - 1 = N - 2$, hence $\text{rk}(A) = N - (N - 2) = 2$. If one now looks at the complete $(k, N - k)$ -bipartite graph, one easily finds two null-eigenspaces of dimension $k - 1$ and $N - k - 1$. This leads to $\text{rk}(A) = 2$. Actually, any rank 2 graph is a complete bipartite graph, as can be shown by looking at A matrices one can build from two orthogonal vectors. Its two non-null eigenvalues of a rank-2 graph are

$$\pm D = \pm \sqrt{\frac{\text{Tr} A^2}{2}} = \pm \sqrt{k(N - k)}. \quad (16)$$

IV. A RESOURCE THEORY OF SQUEEZING

The Gaussian bosonic states of subsection II A are of particular significance in the theory of continuous variable quantum information, in particular in their quantum optical implementations. They are in fact resources for measurement based quantum computing [32, 34], quantum simulations [22], multi-party quantum communication [21, 36], and quantum metrology [37, 38].

Being interested in the nature of the correlations between such states, the first moments become irrelevant. In any practical realization of a quantum computation or

² In general, any CV graph can be reshaped in any other graph via a symplectic transformation; in this case it is an orthogonal transformation, and its physical realization involves only linear optics without any supplementary squeezing.

communication protocol with Gaussian states, first moments do play a role, but these are normally managed in the post-processing and do not interfere with the dynamics of the second moments. We can thus assume that our quantum states are fully described by their covariance matrix.

We have seen in the previous section that the squeezing is the essential resource for building Gaussian entangled states. A natural question is thus: what is the squeezing cost of producing a quantum state?

A general resource theory for Gaussian states is provided in [39]. The specific case of squeezing is described in [40] where they show an operational squeezing measure for any symplectic transformations S :

$$F : \mathbb{R}^{2N \times 2N} \rightarrow \mathbb{R}, \quad F(S) = 20 \sum_{i=1}^N \log_{10} \left(\sqrt{\lambda_i^+(S)} \right), \quad (17)$$

where $\sqrt{\lambda_i^+(S)}$ are the largest singular values of S , while \log_{10} and the factor 20 ensures that the outcome is measured in dB . Using eq. (3), we can then define a squeezing measure for covariance matrices

$$G : \mathbb{R}^{2N \times 2N} \rightarrow \mathbb{R}, \quad G(\sigma) = \sum_{i=1}^N 10 \log_{10} (\lambda_i^+(2\sigma)) \quad (18)$$

Where we multiplied the covariance matrix σ by 2 so that the vacuum state has a vanishing cost. This definition can be generalized for arbitrary quantum states, but assumes this particularly simple form for pure Gaussian ones and it works for any number of modes. We will employ it to classify networks topologies, basing on how their squeezing cost scales with the dimension of the network. This is perfectly justified for the implementation strategies that in section II A we have defined of type i), i.e. tailored multimode down-conversion processes [19, 21, 25–28], where the experimental challenge is due to the trade-off between the number of modes and the amount of squeezing in each mode, both of which are considered by the resource theory. In other kind of experimental scenarios, such as time-multiplexed regular graph states implementation [16, 17], where few squeezers are used to create the network by the interference of delayed squeezed pulses, the main limitation is due to the amount of squeezing in each mode, which can be easily obtained from G if we divide by the number of squeezed modes. As a matter of fact, any resource theory should be tailored to the specific experimental scenario under consideration and eq. (18) provides a versatile tool for this purpose.

V. SQUEEZING COST FOR NETWORK GENERATION

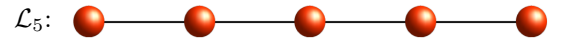
In this section we apply the results presented above to various topologies of Gaussian networks, to study how their squeezing requirement scales with the size of the network depending on its own structure. As stated in the first section, a node in the network is a pure continuous variables Gaussian state, that will be called a qumode,

and is completely defined by its own covariance matrix. In the following, we will consider an initial set of N modes vacuum states with no squeezing ($s = 0$), as it can be easily proved that initial uniform squeezing only adds a constant factor to the final squeezing cost. We also assume that the CZ-gate coupling strength $g = 1$ for every edge of the graph, keeping the effects of non-uniform correlations for future works.

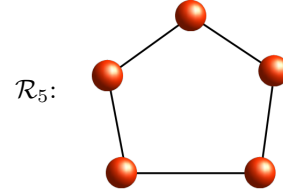
A. Regular Networks

Let us first discuss some regular network structures. We shall consider the following topologies:

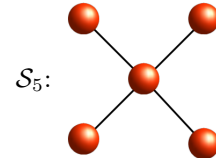
- The *linear graph* \mathcal{L}_N , with N nodes and $N - 1$ edges, is accomplished by connecting each node in series to the next.



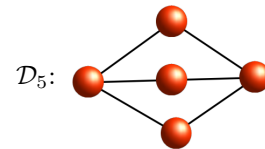
- The *ring graph* \mathcal{R}_N , with N nodes and N edges, is a linear graph with a closed loop.



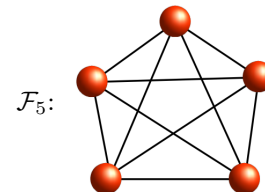
- In the *star graph* topology \mathcal{S}_N , with N nodes and $N - 1$ edges, every peripheral node is linked to a central node, called hub.



- The *diamond graph* \mathcal{D}_N , with N nodes and $2(N - 2)$ edges, has 2 hubs, each linked to all the $N - 2$ central nodes of the network. It is isomorphic to the complete bipartite graph in which one of the subset has 2 nodes and the other has $N - 2$ nodes.



- In the *complete* (or *fully connected*) graph \mathcal{F}_N , with N nodes and $\frac{N(N-1)}{2}$ edges, all nodes are interconnected.



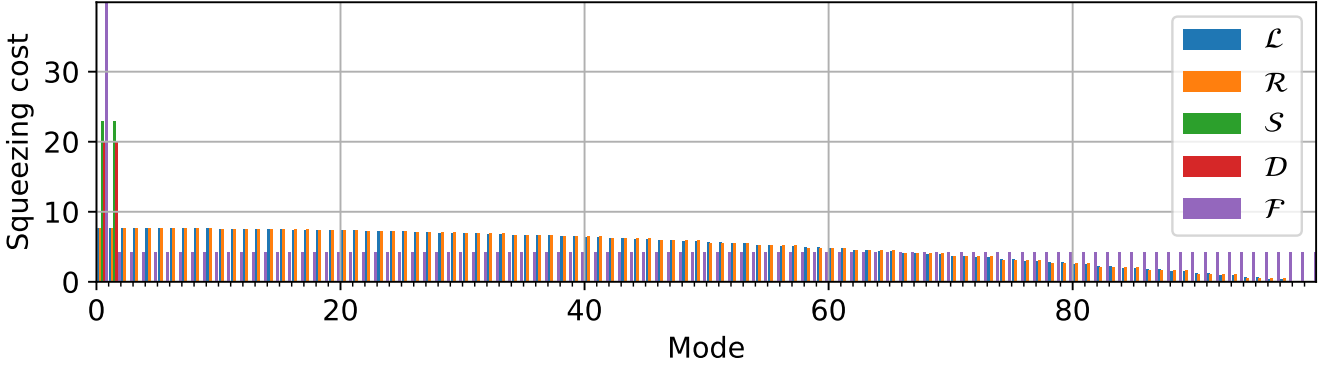


FIG. 1: Squeezing cost distribution for regular networks: linear \mathcal{L}_N , ring \mathcal{R}_N , star \mathcal{S}_N , diamond \mathcal{D}_N , fully connected \mathcal{F}_N networks in the $N = 100$ supermodes, $s = 0, g = 1$. All the networks present some squeezing in each mode except the \mathcal{S} and \mathcal{D} that have an equal amount of squeezing only in the first two modes. The \mathcal{F} network has a large peak of squeezing in the first mode, while the remaining amount of squeezing is equally distributed in the other modes.

Let us first take a look at the full squeezing spectrum of these topologies for a fixed number of nodes $N = 100$. This is shown in figure 1, where the values were computed starting from the adjacency matrix spectrum of regular graphs [41]. We can see that, as expected, the linear and the ring graphs have a very similar spectrum, with small deviations induced by the periodicity of the latter that becomes negligible for large N . The star and the diamond networks only have two squeezed modes for all N . They are thus co-spectral up to a factor and can be transformed the one into the other with linear optics. Finally, the fully connected graph has one large eigenvalue that grows with N and $N - 1$ uniform eigenvalues that are constant with the size of the graph.

Let us now see how the total squeezing cost $G(\sigma)$ scales with the number of nodes N for each of the network topologies presented above. The analytical expressions for all these graphs are shown in appendix A. In Fig. 2 we

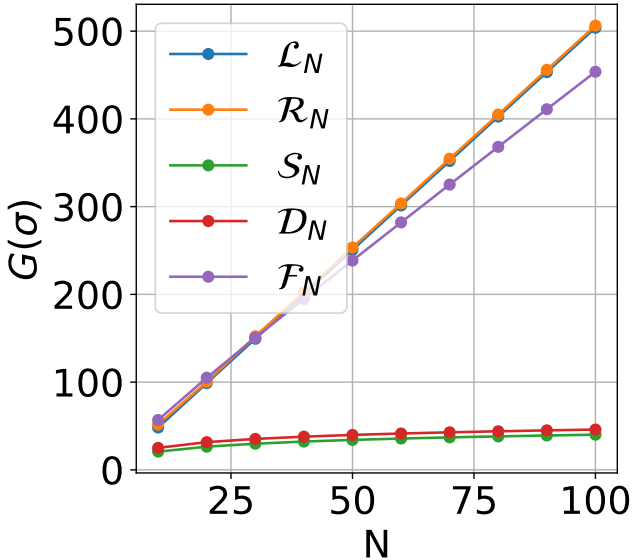


FIG. 2: Trend of the squeezing cost $G(\sigma)$ for the regular topologies: linear \mathcal{L}_N , ring \mathcal{R}_N , star \mathcal{S}_N , diamond \mathcal{D}_N , fully connected \mathcal{F}_N networks for $N = 100$ nodes.

can see how the linear graph in blue and the ring graph

in orange are superposed, sharing the same squeezing cost per node that, as shown in appendix A, is constant with N . The cost of the star and diamond grows logarithmically with N and in both cases has a simple expression and present the lowest cost among the regular graphs we studied. In all these cases, although the actual squeezing cost would be smaller for these networks, the amount of squeezing required in each mode is much larger so, depending on the experimental scenario, their implementation could be the easiest or the most challenging from an experimental point of view. In any case, these networks have interesting applications for quantum communications. In particular, the star graph can be used for secret sharing [21], while the diamond produce an effect that we called *parallel enhancement of entanglement*, which will be explained in the next section. Finally, the fully connected graph, has a cost that grows linearly with N and, despite having the largest number of edges and thus of squeezing increasing operations, for a large number of nodes is slightly cheaper than the linear graph.

Notice that there is as well a simple relation between the adjacency matrix of a graph state and the energy difference between the state and the vacuum. In fact, assuming that the energy E of the state is the mean value of the harmonic oscillator Hamiltonian on the state

$$E = \langle \hat{H}_{HO} \rangle = \frac{\hbar}{2} \sum_i \omega_i (\langle \hat{x}_i^2 \rangle + \langle \hat{p}_i^2 \rangle) = \frac{\hbar\omega}{2} \text{Tr}(\sigma), \quad (19)$$

where we also assumed that all the modes have the same frequency $\omega_i = \omega$. From this we can write

$$\Delta E = E - E_0 = \frac{\hbar\omega}{2} \text{Tr}(\sigma - \sigma_0) = \frac{\hbar\omega}{2} \text{Tr}(A^2). \quad (20)$$

The quantity on the right hand-side is proportional to the second moment of the eigenvalues distribution and it sets a fundamental lower bound on the energy necessary to implement such states. From a topological point of view, the trace of the n -th power of the adjacency matrix equals the number of closed loops of length n on the graph [42]. Thus, for $n = 2$, it corresponds to the number of edges in the network and implies that each independent application of the CZ-gate adds the same amount of energy. A resource scaling that is linear with

the number of edges in the network is typical of DV networks (i.e. DV graph states), where each new edge requires a new Bell pair. The scaling of the squeezing in CV networks with the size of the network, as we have seen, depends instead on the structure of the underlying graph and can be non-linear with the number of edges. We want to stress here that squeezing –and not energy– is the technologically not-trivial enabling resource to be implemented for building the CV networks. If we look again at the example of the star and the diamond graph, the number of edges in the two graphs are different, hence they would have different energies. As they have the same number of squeezed mode, we can transform one into the other with passive optics, e.g. without spending energy. However, it has to be clarified that the two main squeezed modes for the diamond have larger eigenvalues than the star network. Thus, if we transform a star graph into a diamond with linear optics, it would be equivalent to a graph state obtained by the application of CZ-gate with a weaker coupling g . But again this behaviour is totally accounted by the squeezing cost, which is the relevant quantity in designing CV networks.

B. Complex Networks

So far we described graphs that are built through a deterministic algorithm, though we can also construct a graph based on statistical models [43, 44]. This is the difference between regular and random networks. An exemplary standard for random networks is the Erdős–Rényi model $\mathcal{G}_{ER}(N, p)$, in which each pair of the N nodes have a probability p to be linked; the network thus has $\binom{N}{2}p$ edges on average [45].

Most of the network properties observed in nature, however, simply cannot be described by regular or random graphs. For this reason, a youthful branch of scientific research is committed to the study of *complex networks*. In the field of network theory, complex networks are a type of graphs with non trivial topological features, that are shared by neither regular nor random graphs, but are rather akin to networks modeling real systems [46].

An important class of complex networks is characterized by the *small world* property. These networks exhibit the peculiarity of having a low average path length, which is the mean distance between two arbitrary nodes, and a high clustering, which is a measure of the degree to which nodes in a graph tend to cluster together. The emblematic network presenting these features is the Watts–Strogatz model $\mathcal{G}_{WS}(N, Q, \beta)$ [47]. In this model, we first construct a regular periodic graph with N nodes and $\frac{NQ}{2}$ edges where each node has exactly Q neighbors, then with probability β we rewire each edge with another node chosen uniformly at random while avoiding self loops and link duplications.

The second relevant class of complex networks present the typical aspect of being *scale-free* and having *long-tailed* structures. Scale-free networks show a power law in the degree distribution $P(k) \propto k^{-\gamma}$ for some $\gamma > 0$, which is self-similar at all values of k in the *tail* of the distribution, unlike the ER and WS models that go to zero very quickly and have no tails. This fractal

like attribute is well reproduced by the Barabási–Albert model $\mathcal{G}_{BA}(N, K)$, which can also emulate growth and preferential attachment in networks [48]. The graph is built sequentially by adding one node at a time and wiring it to K other nodes with a probability that is proportional to the number of links that the target node already has. While adding one node at a time, the first K nodes initially will not be linked to anything, hence this graph will result having $(N - K)K$ edges, mostly connected to a great hub. This type of graph is the canonical example to reproduce some properties of the *World Wide Web*. A particular case of the Barabási–Albert network is the *Tree-graph* $\mathcal{G}_T(N) = \mathcal{G}_{BA}(N, 1)$.

Another notable class of complex networks is constituted by *technological networks*, artificial networks designed typically for distribution of some merchandise or resource, such as electricity or information. The most famous example in this category is the Internet Autonomous System (AS) $\mathcal{G}_{AS}(N)$, the physical global computer data network. In order to study this topology we will base on the work put forward in ref. [49]. All the complex networks mentioned so far are meant to emulate man-made structures, however complex topologies appear in nature in the most surprising ways. There is a large variety of *biological networks*, among these we will consider specifically the protein–protein interaction network model $\mathcal{G}_{PP}(N, \sigma)$ developed in ref. [50].

CV quantum networks with complex networks shapes are particularly relevant for simulating quantum complex networks environments [22, 51] and to study future quantum information/communication networks mimicking the structure of the classical communication networks. It is then worth to study the scaling of the necessary squeezing resources for their implementation. In Fig. 4 we show the squeezing cost distribution for the various topologies of complex networks by showing the squeezing cost of all the principal modes. Notice that, since complex networks are a subset of correlated random networks, one cannot find the exact eigenvalues distribution of the adjacency matrix. In some selected cases, however, the eigenvalues follow a known probability distribution $f(x)$ [52], which can be used to derive the expectation value of the total squeezing cost as

$$\langle G(\sigma) \rangle = 10N \int f(x) \log_{10}[\lambda^{(+)}(x)] dx, \quad (21)$$

where $\lambda^{(+)}(x)$ is the largest symplectic eigenvalue of eq. (12) for a real random variable x . This gives us a straightforward recipe to compute G from the distribution f . Furthermore, it allows us to deduce the scaling of G from the distribution of the eigenvalues and especially from the width of this distribution. In fact, if the distribution does not change with N , then G scales linearly with N , whereas any growth in the width of f would imply a superlinear scaling of G . The protein and internet networks, which are scale free networks, have the additional property of having many nodes sharing the same neighborhood which implies a large kernel of their adjacency matrix and thus a slower growth of G compared to the other complex graphs, which are essentially full rank. More specifically, the low rank of the protein–protein interaction graph [50], is explained by

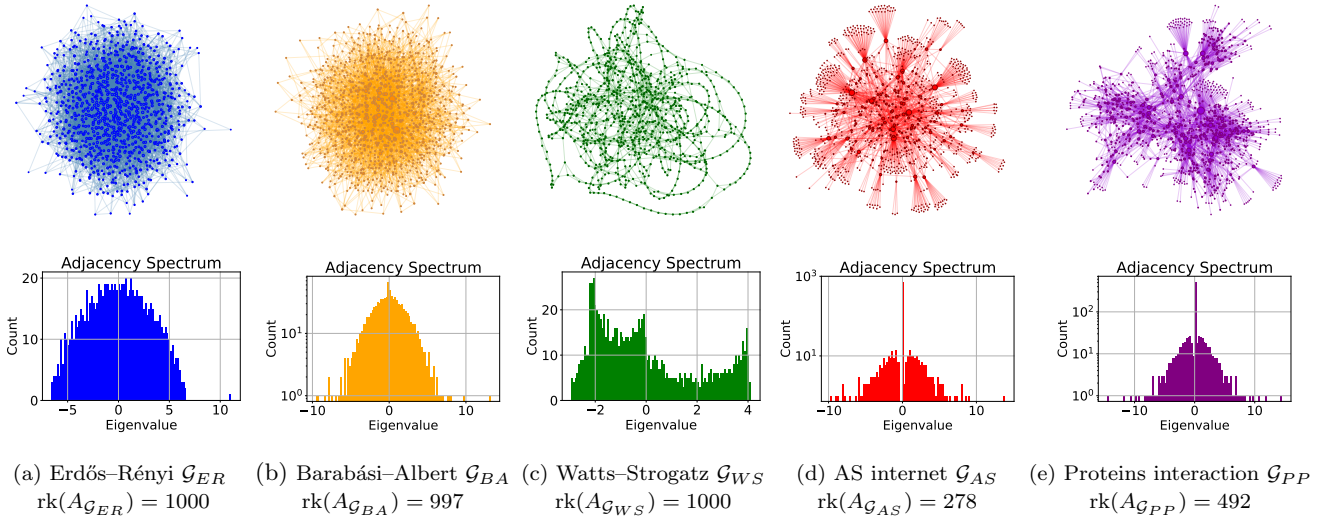


FIG. 3: Some complex networks, their adjacency matrix eigenvalues distribution and the rank of their adjacency matrix for $N = 1000$ nodes. In the distributions of the BA, AS and PP the y-axis is in log-scale.

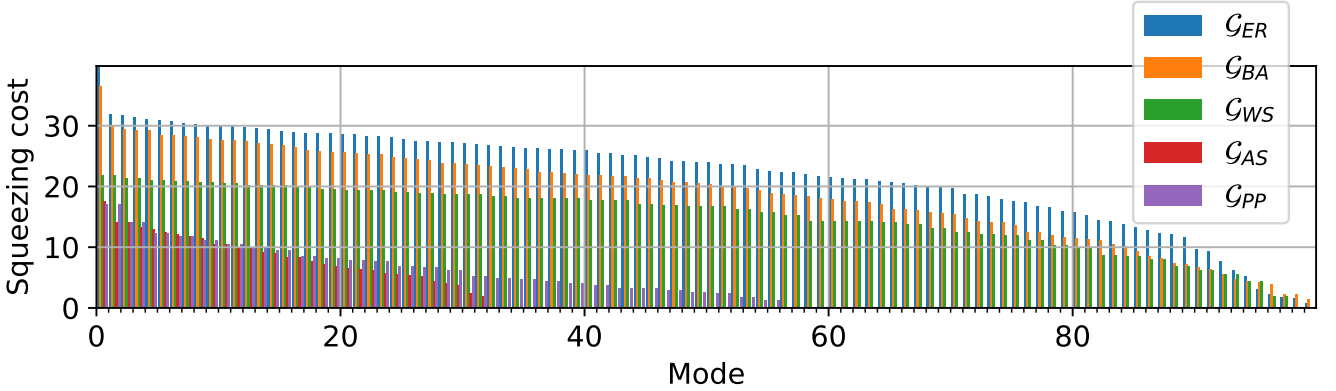


FIG. 4: Squeezing cost distribution for complex topologies: Erdős-Rényi \mathcal{G}_{ER} , Barabási-Albert \mathcal{G}_{BA} , Watts-Strogatz \mathcal{G}_{WS} , AS internet \mathcal{G}_{AS} and Protein-Protein interaction \mathcal{G}_{PP} networks in the $N = 100$ supermodes.

the duplication process at the heart of its generation, which, by definition duplicates the neighborhood of vertices. For the internet graph of [49], in particular, many of the nodes are leafs (clients) connected to a few client providers. This results in a very low –but still linearly increasing with N – rank, explaining why its squeezing cost is the lowest of the line in Fig. 5.

In Fig. 5 we report the trend of the total squeezing cost as a function of the number of nodes for each of the above complex topologies. In this case, the networks were simulated and the values obtained were averaged over ten different samples.

From the plots we notice that the linear trend is the most common case. The spectral theory of real graphs is a much less established field and there is only a handful of results we can apply to actually make predictions. In particular, to the best of our knowledge there are only empirical results about the convergence of the spectral density for the scale-free and the small-world models. In Ref. [52], however, they show some crucial properties of the spectra of scale-free and small-world graphs, although further studies are required in order to have a deeper insight in the properties of complex quantum graph states.

In particular, it is shown that, fixing the other network's parameters, the width of their distribution is constant with N , implying as we discussed a linear trend of G .

The WS graph interpolates between a regular periodic graph and the random graph when the rewiring probability β goes from 0 to 1. In particular, for $\beta = 1$ we have approximately an ER with $p = \frac{Q}{N-1}$, although this model does not approach the actual ER graph since every node will be connected to at least $\frac{K}{2}$ other nodes.

From Fig. 5 we also notice that the most expensive growth belongs to the ER topology, which is the only one among the topologies we studied whose trend is superlinear. This behaviour is actually the easiest to predict from random matrix theory: the Wigner semi-circular law for the distribution of the eigenvalues of a random graph [53] gives their probability distribution in the form $f(x) = f_{ER}(x) = \frac{2}{\pi R^2} \sqrt{R^2 - x^2}$ (see Fig. 3a), where $R = 2\sqrt{Np(1-p)}$. Casting it in equation (21) gives

$$\begin{aligned} \langle G(\sigma_{ER}) \rangle &= 10 \log_{10}[\lambda^{(+)}(pN)] \\ &+ \frac{40N}{\pi R^2} \int_0^R \sqrt{R^2 - x^2} \log_{10}(\lambda^{(+)}(x)) dx, \end{aligned} \quad (22)$$

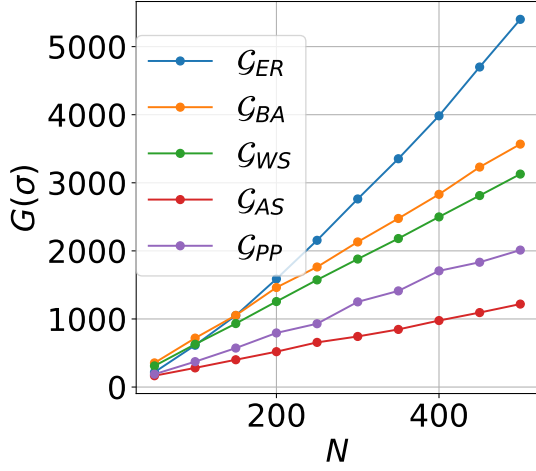


FIG. 5: Trend of the squeezing cost for complex topologies: Erdős-Rényi \mathcal{G}_{ER} , Barabási-Albert \mathcal{G}_{BA} , Watts-Strogatz \mathcal{G}_{WS} , AS internet \mathcal{G}_{AS} and Protein-Protein interaction \mathcal{G}_{PP} networks up to $N = 500$ nodes.

where we used the parity of $f_{ER}(x)$, the fact that the support is in $[0, R]$ and that for the largest eigenvalue, $\lim_{N \rightarrow \infty} \lambda_1/N = p$, with probability 1. Figure 6 shows the comparison between the theoretical behaviour of the squeezing cost of the ER graph and the numerical experiments from the simulations. It shows a superlinear $\propto N \log N$ increase of the squeezing cost, which is explained by the widening of the support of f due to the increasing values of R . More formally, making the variable change $x = Ry$, we have

$$\log_{10} \left(\lambda^{(+)}(Ry) \right) = 2 \log_{10} R + \log_{10} \frac{y^2}{2} + O \left(\frac{1}{R^2 y^2} \right). \quad (23)$$

The second term in eq. (22) then becomes

$$\begin{aligned} \frac{40N}{\pi} \int_0^1 \sqrt{1-y^2} \log_{10} \left(\lambda^{(+)}(Ry) \right) dy \\ = \frac{80N \log_{10}(R)}{\pi} \int_0^1 \sqrt{1-y^2} dy + O(N) \\ = 10N \log_{10}(Np(1-p)) + O(N), \end{aligned} \quad (24)$$

and is the dominant term in the squeezing cost.

Now that we have characterized the cost of implementing Gaussian quantum networks, we will describe how to use them as a substrate to perform quantum communications.

VI. QUANTUM TELEPORTATION GAUSSIAN NETWORKS

Quantum entanglement is a paramount resource for quantum information purposes. In particular, bipartite entanglement represents the fundamental requirement that a shared quantum channel should have in order to enable a truly quantum teleportation. In the framework of Quantum Communications, the networks previously described can be seen as distributed Gaussian *quantum teleportation networks* [54], where each pair of nodes can

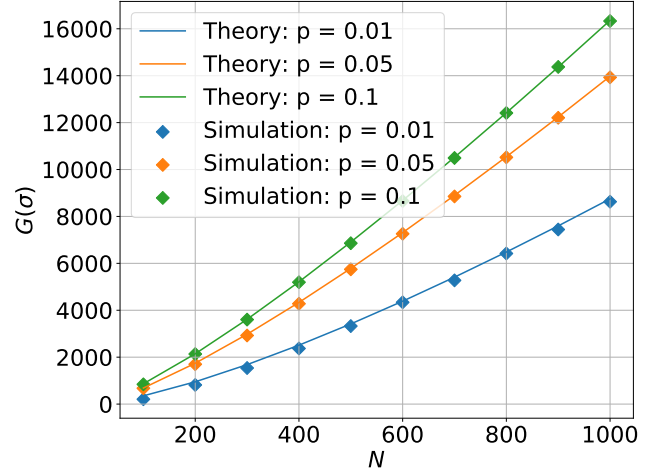


FIG. 6: Comparison between the theoretical prediction of equation (21) and the experimental numerical simulation of the squeezing cost of the Erdős-Rényi graph state, for different values of p .

employ the pre-established quantum correlations together with *Local Operations* and *Classical Communications* LOCC to teleport a Gaussian quantum state from one node to the other.

In a naïve strategy, the teleportation between two arbitrary nodes can be implemented simply by ignoring all the other nodes and exploiting the residual bipartite entanglement together with classical communications. This strategy is a direct extension of the standard teleportation protocol from two to more stations and is called *non-assisted* protocol [55].

Another set of strategies is based upon a cooperative behavior, where all the other nodes assist the teleportation between the chosen pair (Alice and Bob) by means of LOCC. In fact, if the external nodes perform suitable local measurements and then classically communicate their outcomes to Bob, the latter can use this additional classical information to improve the process via modified conditional displacements. These strategies are called *assisted* protocols and are the ones that determine what we call networking/routing protocol in this Article.

According to Gu et al. [34] quadrature measurement on a mode of a Gaussian network like the ones we considered so far can be described by two simple rules:

- *Vertex Removal*: a \hat{q} -measurement on a qumode removes it from the network, along with all the edges that connect it.
- *Wire Shortening*: a \hat{p} -measurement on a qumode is just a \hat{q} -measurement after a Fourier Transform, which corresponds to a phase rotation of $\pi/2$: $S_F = S_R(\theta = \frac{\pi}{2})$. The node will thus be removed but the phase shift will induce correlations between the neighbouring edges. Thus, measurements in the momentum basis allow us to effectively “shorten” linear graph states.

If two nodes A and B need to teleport a quantum state, they can be helped by the other nodes in the network who will perform these operations in order to increase the

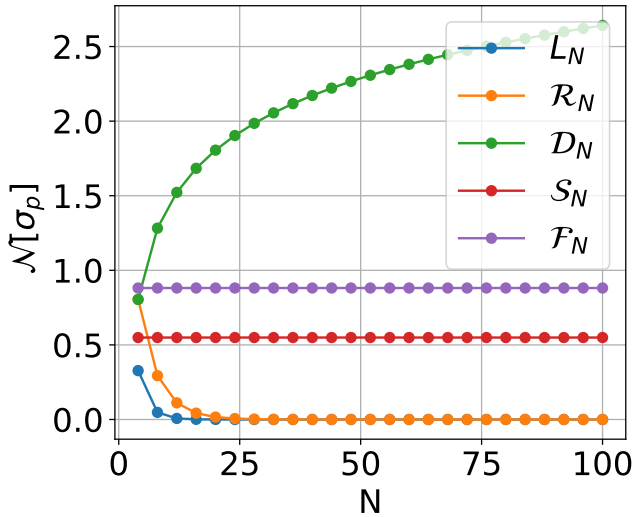


FIG. 7: Negativity in the final two modes states after that all the other agents have locally measured their node for the regular topologies: linear \mathcal{L}_N , ring \mathcal{R}_N , star \mathcal{S}_N , diamond \mathcal{D}_N , fully connected \mathcal{F}_N networks up to $N = 100$ nodes.

strength of the entanglement in the final pair. A typical measure of entanglement is the *negativity*

$$\mathcal{N} = -2 \log_2 \nu_- \quad (25)$$

Where ν_- is the smallest symplectic eigenvalue of the partially transposed covariance matrix of the pair. Partial transposition is a necessary operation for the PPT criterion [56] and is easily implemented in Gaussian states by changing the sign of the momentum of one of the two subsystems. For Gaussian states, the negativity is simply connected to another measure of entanglement, the fidelity of teleporting a coherent state through that quantum channel

$$\mathcal{F}_{\text{coh}} = \frac{1}{1 + \nu_-} \quad (26)$$

Simple classical communication attains at most $\mathcal{F}_{\text{coh}} = \frac{1}{2}$ so a bipartite system presents truly quantum correlations only if $\mathcal{F}_{\text{coh}} > \frac{1}{2}$, or equivalently $\nu_- < 1$ and $\mathcal{N} > 0$.

The symplectic eigenvalues ν_{\pm} of a two-mode system can be computed through the invariants of the covariance matrix [57]. More specifically, we can define the *seralian* $\Delta = \det \sigma_A + \det \sigma_B + 2 \det \sigma_{AB}$, where σ_A and σ_B are the local covariance matrices of the single-mode sub-systems A and B, and σ_{AB} represents their correlations. From this we can compute the symplectic eigenvalues as:

$$\nu_{\pm}^2 = \frac{\Delta \pm \sqrt{\Delta^2 - 4 \det \sigma}}{2} \quad (27)$$

In Fig. 7 we compare the effect of different regular topologies of quantum networks with the purpose of distributing entanglement between two of the furthest nodes inside the network.

The simplest cases are the *star* and *complete* networks. In the first case the best *assisted* strategy is to let everyone perform a \hat{q} -measurement on their node except the central one who will make a *wire shortening* to link

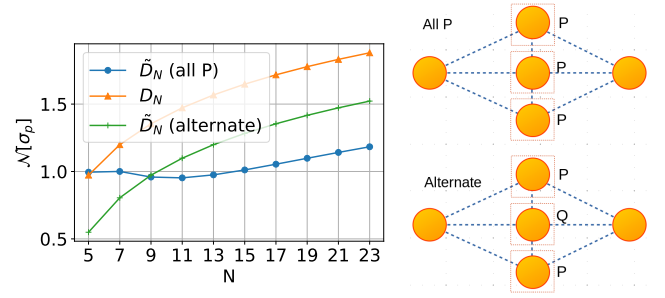


FIG. 8: Different measurement strategies for two types of diamond network: the standard \mathcal{D}_N we have seen so far and the $\tilde{\mathcal{D}}_N$, in which the central nodes are connected to their neighbors. We apply two different strategies to $\tilde{\mathcal{D}}_N$: one is to measure all the central nodes in P and the other is to alternate a p and a q measurement. We can see that measuring always in p is not necessarily the optimal strategy. On the right side you can see a scheme of the $\tilde{\mathcal{D}}$ network and the two different measurement strategies.

the final pair. In the complete network A and B are already linked by an edge so it is sufficient to measure the position in all the other qumodes (notice that this strategy outperforms the non-assisted protocol). In both these cases the entanglement is constant with the number of nodes in the network as we would expect, and the wire shortening of the central node in the star graph decreases the negativity with respect to the complete graph [58]. In the linear graph all the nodes have to wire shorten from A to B. Here the negativity quickly decreases with the number of nodes. The decrease of entanglement with the wire shortening seem to be typical in all configurations except the diamond graph, where all the central nodes are \hat{p} -measured.

VII. MULTI-PATH ENTANGLEMENT

The behaviour of the diamond graph is quite counter-intuitive and might be expected to increase the fidelity of quantum communications. It can be shown (proof in Appendix C) that the lowest symplectic eigenvalue for this system goes like

$$\left(\nu_-^{(\mathcal{D}_N)}\right)^2 = \frac{1}{1 + 2NRg^2}, \quad (28)$$

Where $R = 10^{s/10}$ is the inverse of the squeezing in \hat{p} , with squeezing factor s in dB . Hence, the negativity grows logarithmically with NRg^2

$$\mathcal{N}^{(\mathcal{D}_N)} = \log_2(1 + 2NRg^2), \quad (29)$$

and the two modes become perfectly correlated in the limit of either infinite squeezing, infinite strength CZ-gate or infinite parallel measurements on \hat{p} .

This property of the Diamond network, however, is not easily generalized to all graphs that present parallel connections and the quest for the optimal measurement strategy in order to improve the final entanglement is by no means trivial. This is the case, for example, of the $\tilde{\mathcal{D}}$ graph shown in Fig. 8, generated by taking the diamond network and add a CZ-gate link between adjacent central

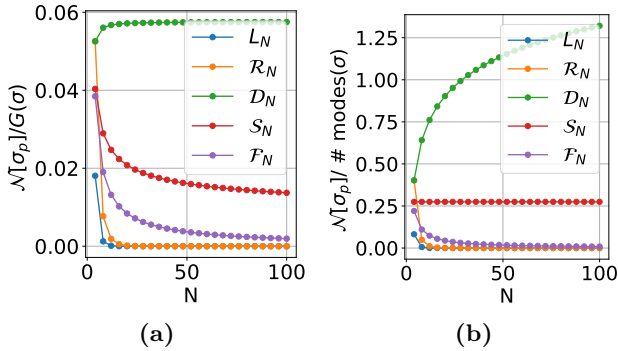


FIG. 9: Trend of the ratio between the negativity of the final state and (a) the squeezing cost of the initial state or (b) the total number of modes in the initial state for regular topologies: linear \mathcal{L}_N , ring \mathcal{R}_N , star \mathcal{S}_N , diamond \mathcal{D}_N , fully connected \mathcal{F}_N networks up to $N = 100$ nodes.

nodes. We can see that for $N > 9$ measuring always \hat{P} in this network is not the optimal strategy, whereas a better strategy is to alternate a \hat{P} and \hat{Q} measurement in order to restore a (smaller) diamond network.

Another important figure of merit is the entanglement per squeezing cost, shown in Fig 9 (a).

We see that the diamond is the only one that gives the a ratio of entanglement per cost of the network that becomes constant for large N . However, the linear graph is the one that links two nodes that are the furthest away from each other. Conversely, figure 9 (b) shows the negativity in the final pair divided by the number of modes in the initial state. Once again, the diamond structure is particularly convenient, yielding the highest negativity while keeping a constant number of independent squeezers.

In order to give a fair comparison between the capacity of the linear network to bridge distant nodes and that of the diamond to increase the final entanglement we need to generalize the diamond graph to a diamond chain graph, $\mathcal{DC}_{K,N}$, where K is the number of parallel branches linking the two hubs that want to perform quantum communications as in figure 10.

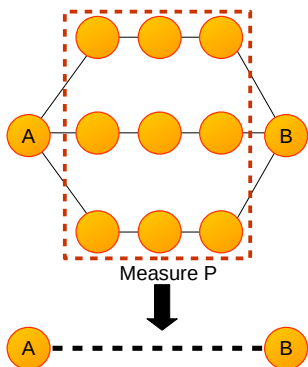


FIG. 10: Scheme of an entanglement routing protocol in a diamond chain with $K=3$. All the central nodes are measured in P in order to concentrate entanglement between Alice and Bob.

We can then compare the entanglement concentrated using multiple path strategies to link two nodes far away from each other. We can see in figure 11 that the presence

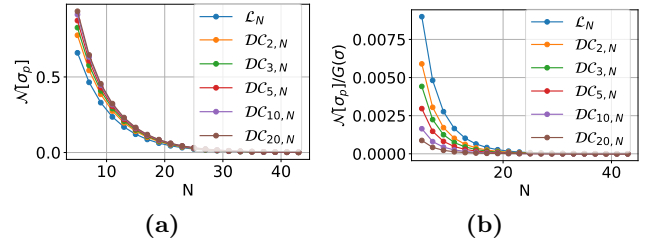


FIG. 11: (a) Trend of the negativity of the output state for the diamond chain network, for various values of the number of branches K ($K=1$ is the linear network). (b) Trend of the ratio between the negativity of the final state and the squeezing cost of the initial state for the diamond chains.

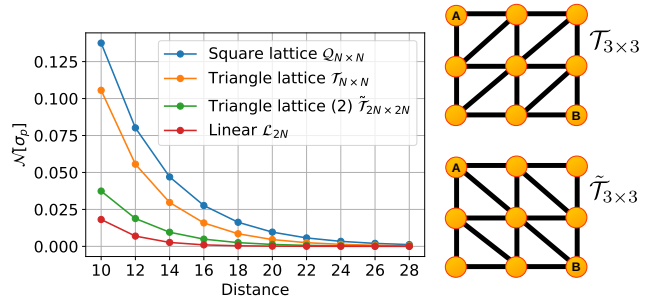


FIG. 12: Comparison between the entanglement capacity between two nodes at the same distance of three lattices graphs, the square lattice $\mathcal{Q}_{N \times N}$ and the two triangles $\mathcal{T}_{N \times N}$, formed from the square by adding edges on the diagonals in such a way that the distance between A and B is the same, $\tilde{\mathcal{T}}_{N \times N}$ formed by adding edges to the diagonals so that the distance is the same as the linear graph, and the linear graph \mathcal{L}_N . In order to compare the networks with the same distance we doubled the size of the $\tilde{\mathcal{T}}$ and the \mathcal{L} graphs.

of parallel links has indeed the desired effect, despite the quality of the final pair, which still decreases exponentially with the distance. On the other hand, notice that the parallel links can help concentrating more entanglement until the system reaches a plateau and even the additional channels will not allow to increase the negativity. Moreover, the value for effort of this networks, specifically the ratio between the entanglement of the pair after the protocol and the squeezing cost before the protocol, is maximized by the linear graph.

Another important class of networks, notably for measurement based quantum computation, is constituted by grid cluster states that belong to graph shapes that allow for universal quantum computation [59]. Similarly to the diamond network, the presence of ancillary nodes between the emitter and the receiver can improve the quality of the quantum link with respect to the linear network. This, however, is not a general rule and sometimes the presence of additional links can be detrimental. This is the case of the triangular lattice, generated from the square lattice by adding a link between the nodes in the diagonal. There are two ways of generating the triangular and only one of the two, $\tilde{\mathcal{T}}$, decreases effectively the distance between Alice and Bob. In both cases the result is detrimental, however \mathcal{T} is slightly better than $\tilde{\mathcal{T}}$, while the square lattice \mathcal{Q} seems to be the most effective. This result is shown in figure 12.

VIII. ROUTING PROTOCOL

In this section we aim at employing the abstract notions on Gaussian graphs developed so far for a specific application: the routing of entanglement. In this scenario, the highly multimode entangled Gaussian state corresponds to a distributed teleportation network, described in the previous section, where each node of the network is supplied with a mode of an electromagnetic harmonic oscillator and is linked to some other nodes in different locations through quadrature correlations, e.g. quantum entanglement. We remark that this type of communication quantum networks is inherently different from the typical qubit networks that are currently being deployed in different metropolitan areas [60]. In those cases, for example, each entanglement link is pairwise between two qubits and as a consequence each node of the network will have to receive, storage and measure as many quantum states as neighbors it has. Conversely, in a Gaussian quantum network the same qumode can be entangled with an arbitrary number of other nodes. Moreover, the production of such states, their manipulation to increase the entanglement among two nodes and their measurement to perform quantum teleportation can be achieved deterministically, unlike the discrete variables case. Nonetheless, qubits networks have been extensively studied over the last years, whereas Gaussian teleportation networks is a very recent emerging field. Our purpose is, thus, not to prove the superiority of the latter, but rather to explore its properties and the differences from the DV schemes in order to get the best of both worlds.

The results of the previous sections, highlighted some outstanding properties of Gaussian networks. The most important is the parallel enhancement of entanglement in the diamond graph. If properly used, this feature can most certainly improve the routing of entanglement in regular and complex shaped networks. On these grounds, the search for an optimal protocol that exploits all the qualities of these Gaussian networks is very desirable yet arduous, and will be subject of future investigations. Alternatively, we present a naïve entanglement routing protocol that takes into account some of these properties and we will apply it to complex topologies, to show that the enhancement of the entanglement with respect to the trivial protocol is, in principle, easily achievable. Imagine we have a distributed network of entangled harmonic oscillators, where each node is honest and can perform classical communication and local homodyne measurement, and we want to establish an entangled pair between two nodes, Alice and Bob, that want to teleport a quantum state or perform QKD. The trivial protocol — called *Shortest* in the following — would be to find the shortest path between them and measure in P all the qumodes along this path and in Q all the others. A careful look at the inner structure of the network, however, might help us increase the strength of the correlation. For example if at any point, two nodes on the path are linked by multiple parallel routes, we can measure these in P to exploit the parallel enhancement.

In order to show this in practice, we will test the performances of three different routing protocols (shown in

figure 13) on various complex networks with the purpose of establishing a highly entangled pair [61]. We choose Alice to be one of the hubs of the graph and evaluate the efficiency of the protocol in delivering entanglement to all the other nodes. The quantum protocol that we propose to exploit the parallel enhancement of entanglement will be simply called *Routing*.

- *Routing*: it takes as input the target node, Bob; it lists all the shortest paths connecting it to Alice and measures all the nodes that are not in these paths in the \hat{Q} quadrature, so that they will not influence the protocol. Among the list of paths it checks one by one those to be measured in \hat{P} in order to maximize the negativity \mathcal{N} of the final pair, while the rest will be measured in \hat{Q} .

In the *Routing* protocol, in principle, we could have considered as well parallel paths of longer lengths that might have contributed to improve the negativity. However, in practice had the only effect of slowing down the performances while not increasing the entanglement for all the cases we considered. The effect of the parallel paths can be appreciated when comparing the negativity produced by *Routing* with that produced by *Shortest*.

- *Shortest*: the difference of the latter is that it only exploits one of the shortest parallel paths, directly measuring everything else in Q .

In some cases the two protocols do not give a substantial difference, either because there are not parallel routes or because these do not help increasing the entanglement, however in many instances the effects of parallel routing are significant. The last protocol we compare with is *All P*.

- *All P*: it measures all the terminal nodes with degree 1 in \hat{Q} and the rest in \hat{P} .

This protocol is less effective than the first two but is always the quickest, whereas *Routing* can be computationally very slow on regular networks, which are characterized by long distances and many parallel paths, but becomes very efficient on complex sparse networks. The following simulations can be reproduced using our python code, available at [61].

One instance of this program is given in figure 14 which shows the negativity provided by the three different protocols for each node of a $\mathcal{G}_{AS}(N = 1000)$ network. At the beginning of the protocol, we pick Alice as the node, or one of the nodes, with the highest degree. The nodes are then sorted by their distance from Alice and, for the same distance, by the number of all the shortest paths connecting them to Alice. Additionally, the grey column represents the ratio of parallel paths that were useful to increase the entanglement. Notice that nodes at distance 1 cannot show a difference between the *Routing* and the *Shortest* protocols, however many nodes at distance 2 present a greater negativity than those at shorter distance after the *Routing*.

In figure 15 we show the graph of the network, where the nodes are again sorted by distance and number of parallel paths and the size of each node is proportional to its degree. In this figure Alice is ‘0’ and has a thick

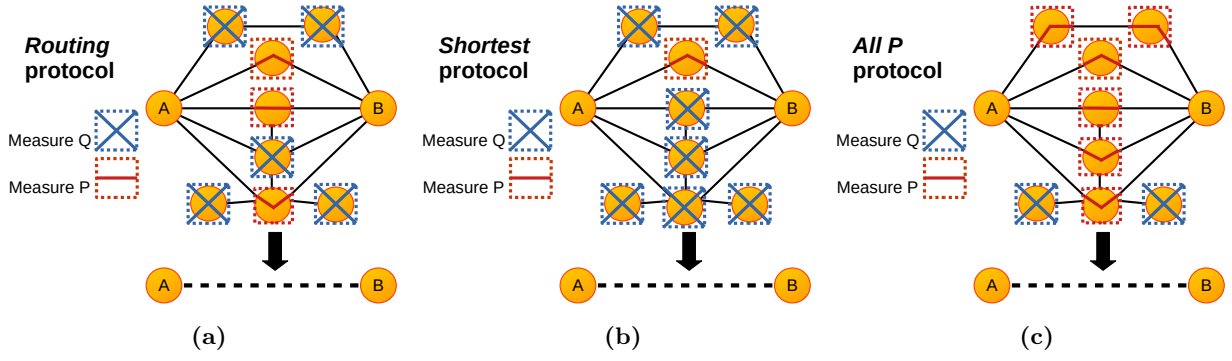


FIG. 13: Scheme of the three protocols for the entanglement distribution: (a) the *Routing* protocol takes a list of the shortest paths connecting A and B and measures in \hat{P} those that increase the negativity while the rest is measured in \hat{Q} ; (b) the *Shortest* protocol only consider one of the shortest paths to be measured in \hat{P} and the rest in measured in \hat{Q} ; (c) the *All P* measures the nodes with only one connection in \hat{Q} and all the rest in \hat{P} .

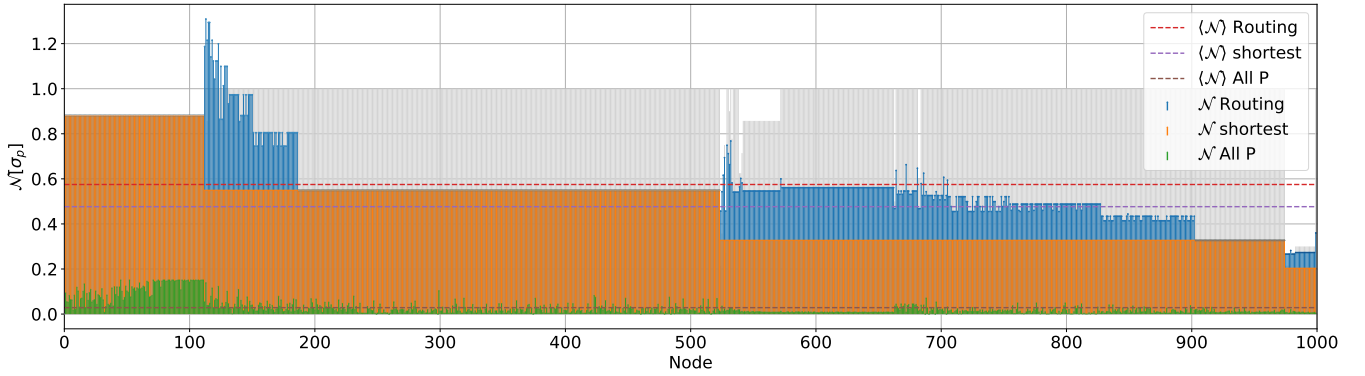


FIG. 14: Negativity produced by the three different protocols applied to each node of the the $\mathcal{G}_{AS}(N = 1000)$ network. The nodes are labeled in order of distance and of number of paths connecting to Alice. The blue, orange and green stems represent the negativity of the final pair after the *Routing*, *Shortest* and *All P* protocols respectively, while the dashed lines represent the mean value for all the nodes. The color of the marker indicates the distance of the node from A and the grey columns represent the ratio of paths that improved the entanglement in *Routing*.

red contour. The node with highest negativity and all the paths that improved its entanglement are highlighted with red thick lines.

The same analysis was done in several networks with different sizes and topologies with very different results that we report in figures 16, 17, 18 and 19. A property that is not apparent in Fig. 15, is that the node with the highest enhancement of entanglement due to the multiple paths is not necessarily the one with the highest negativity in absolute. This is the case of the ER network of Fig. 16, in which the node with the highest entanglement, highlighted in green in the graph representation, is at distance 1 while the node with the highest difference in negativity between the *Routing* and the *Shortest* protocols, highlighted in red, is at distance 3. In this case, the structure of the subgraph used throughout the *Routing* is not a diamond chain and the intercorrelations among the parallel branches have limited the increase of the entanglement, as for the \hat{D}_N network in Fig. 8. In any case, in this network the nodes at greater distances are the ones that are most affected by our protocol and, although in some cases many parallel paths have been disregarded, as shown by the height of the grey column, all the nodes at distance 4 received a substantial enhancement.

The results of the simulation on the BA topology of Fig.

17 is similar to the AS, although the first only reaches a distance of 3. The nodes with the highest absolute negativity and the highest negativity difference produced by the *Routing* protocol coincide and are at distance 2 from Alice, whereas this time the subgraph of is a diamond with no interconnections. Also in this case distance 2 is favorable to perform quantum communications.

The WS structure of Fig. 18, on the other hand, is the worst to apply the *Routing* protocol. Only a few nodes, in fact, were poorly enhanced and mostly at large distances, while the negativity averaged over all the nodes for *Routing* and *Shortest* is comparable. The node 44 at distance 3 is the one that received the greatest boost from our protocol, whereas node 1 (like all the other nodes at distance 1) has the highest negativity.

Finally, the biological network of Fig. 19 produced the most interesting results. Once again, many nodes at distance 2 end up having more negativity than those at distance 1, and at this distance the nodes with the same degree have the same negativity that decreases exponentially with their degree. The nodes with highest negativity and highest difference coincide with node 139, which is linked to Alice through 33 intermediate nodes, forming a diamond network with no interconnections.

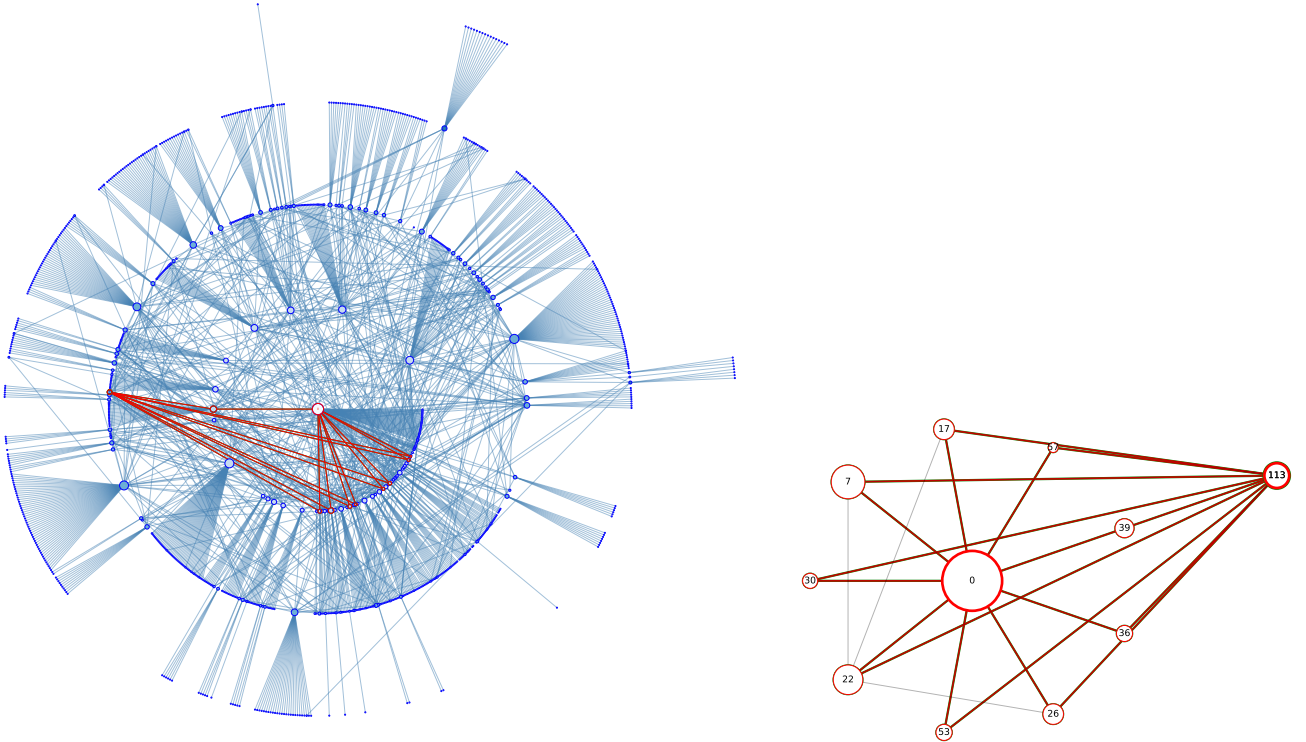


FIG. 15: Scheme of the $\mathcal{G}_{AS}(N = 1000)$ network on which we performed the protocol and subgraph of the paths connecting to the node with highest negativity. The nodes are set in circles according to their distance from Alice and their size is proportional to the degree.

IX. CONCLUSION AND OUTLOOK

A. Conclusion

We have studied Gaussian multimode quantum networks with regular and complex topologies for quantum communication protocols. In particular: i) we have studied their cost in term of amount of squeezing and number of necessary squeezed modes to build the network; ii) we have established a multi-path routing protocol distributing entanglement between two arbitrary nodes. In details:

- We have shown analytically and numerically that the cost of the networks is in general nonlinear with the number of edges and nodes and there are particular (regular and complex) graph shapes that optimize the cost and the number of squeezers over number of nodes/edges in the networks. Among regular networks the diamond and the star graph need only two squeezed nodes to be built, independently from their number of nodes. Among the complex networks shapes, the Internet Autonomous System model is the most convenient in number of needed squeezed states.
- We have studied the assisted teleportation protocol in Gaussian entangled networks, where couple of nodes are assisted in the teleportation by local measurement in all the other nodes. This naturally define a routing protocol in Gaussian networks. In particular we have considered \hat{Q} and \hat{P} homodyne quadrature measurement that allow respectively for

vertex-removal and wire-shortening.

- The routing is optimized by different measurement schemes in regular networks. In the linear and the diamond networks the best strategy consists in the wire shortening, but the diamond network shows the largest ratio in reached entanglement over cost.
- Inspired by the behaviour of the diamond network we have devised a routing protocol that exploits wire shortening in parallels paths and we have applied it to complex networks graphs. The protocol named *Routing* is compared with *Shortest*, where wire shortening is done only in the shortest path, and *All P*, which removes all the terminal nodes while it wire-shorten all the others. In most cases, the *Routing* improves the entanglement compared with *Shortest*. Also, in terms of computational complexity, the *Routing* is much slower than *All P* in regular networks, where there are long distances between nodes and several parallel paths, but it is very efficient in complex sparse networks.

B. Outlook

The devised *Routing* protocol is very general so that it can be applied to arbitrary networks, and it is particularly efficient for sparse not regular networks. Our simple graph exploration approach would be improved in computational efficiency by real graph-based algorithms, especially if we allow for approximate solutions. [62]. Also it would be interesting to allow for non uniform

distributions of squeezing s and CZ gate strength g or more general homodyne measurements, i.e. going beyond the two \hat{P} and \hat{Q} cases and considering measurements along $\hat{Q}_\theta = \cos(\theta)\hat{Q} + \sin(\theta)\hat{P}$. In addition, it could be interesting to examine a scenario in which the intermediate nodes are dishonest and do not cooperate to perform the routing. Moreover, in order to consider practical implementations, realistic parameters for losses and noise should be included in the model. Finally the routing protocol has been implemented to solve the particular task of creating a perfect EPR pair between two nodes, fu-

ture protocols will consider general reshaping in arbitrary multiparty states.

X. ACKNOWLEDGEMENTS

We thank Dimitrios Tsintasilidas for helpful discussions. This work was supported by the European Research Council under the Consolidator Grant COQCOON (Grant No. 820079)

-
- [1] S. Wehner, D. Elkouss, and R. Hanson, “Quantum internet: A vision for the road ahead,” *Science*, vol. 362, no. 6412, 2018.
 - [2] M. Pant, H. Krovi, D. Towsley, L. Tassiulas, L. Jiang, P. Basu, D. Englund, and S. Guha, “Routing entanglement in the quantum internet,” *npj Quantum Information*, vol. 5, no. 1, p. 25, 2019.
 - [3] X. Guo, C. R. Breum, J. Borregaard, S. Izumi, M. V. Larsen, T. Gehring, M. Christandl, J. S. Neergaard-Nielsen, and U. L. Andersen, “Distributed quantum sensing in a continuous-variable entangled network,” *Nature Physics*, vol. 16, no. 3, pp. 281–284, 2020.
 - [4] S. L. Braunstein and P. Van Loock, “Quantum information with continuous variables,” *Reviews of modern physics*, vol. 77, no. 2, p. 513, 2005.
 - [5] F. Hahn, A. Pappa, and J. Eisert, “Quantum network routing and local complementation,” *npj Quantum Information*, vol. 5, no. 1, pp. 1–7, 2019.
 - [6] W. Kozłowski, A. Dahlberg, and S. Wehner, “Designing a quantum network protocol,” in *Proceedings of the 16th International Conference on emerging Networking EXperiments and Technologies*, pp. 1–16, 2020.
 - [7] Y. Zhong, H.-S. Chang, A. Bienfait, É. Dumur, M.-H. Chou, C. R. Conner, J. Grebel, R. G. Povey, H. Yan, D. I. Schuster, *et al.*, “Deterministic multi-qubit entanglement in a quantum network,” *Nature*, vol. 590, no. 7847, pp. 571–575, 2021.
 - [8] H. Leone, N. R. Miller, D. Singh, N. K. Langford, and P. P. Rohde, “QuNet: Cost vector analysis and multi-path entanglement routing in quantum networks.” arXiv:2105.00418.
 - [9] C. Meignant, D. Markham, and F. Grosshans, “Distributing graph states over arbitrary quantum networks,” *Phys. Rev. A*, vol. 100, p. 052333, Nov 2019.
 - [10] C. Meignant, D. Markham, and F. Grosshans, “Classical-quantum network coding: a story about tensor.” arXiv:2104.04745.
 - [11] B. Zhang and Q. Zhuang, “Entanglement formation in continuous-variable random quantum networks,” *npj Quantum Information*, vol. 7, no. 1, p. 33, 2021.
 - [12] Q. Zhuang and B. Zhang, “Quantum communication capacity transition of complex quantum networks,” *arXiv preprint arXiv:2011.07397*, 2020.
 - [13] Y. Omar, J. Moutinho, A. Melo, B. Coutinho, I. Kovacs, and A. Barábasi, “Quantum link prediction in complex networks,” in *APS March Meeting Abstracts*, vol. 2019, pp. R28–003, 2019.
 - [14] M. Cuquet and J. Calsamiglia, “Limited-path-length entanglement percolation in quantum complex networks,” *Physical Review A*, vol. 83, no. 3, p. 032319, 2011.
 - [15] F. Hahn, A. Pappa, and J. Eisert, “Quantum network routing and local complementation,” *npj Quantum Information*, vol. 5, no. 1, p. 76, 2019.
 - [16] W. Asavanant, Y. Shiozawa, S. Yokoyama, B. Charoensombutamon, H. Emura, R. N. Alexander, S. Takeda, J.-i. Yoshikawa, N. C. Menicucci, H. Yonezawa, *et al.*, “Generation of time-domain-multiplexed two-dimensional cluster state,” *Science*, vol. 366, no. 6463, pp. 373–376, 2019.
 - [17] M. V. Larsen, X. Guo, C. R. Breum, J. S. Neergaard-Nielsen, and U. L. Andersen, “Deterministic generation of a two-dimensional cluster state,” *Science*, vol. 366, no. 6463, pp. 369–372, 2019.
 - [18] J. Roslund, R. M. De Araujo, S. Jiang, C. Fabre, and N. Treps, “Wavelength-multiplexed quantum networks with ultrafast frequency combs,” *Nature Photonics*, vol. 8, no. 2, p. 109, 2014.
 - [19] M. Chen, N. C. Menicucci, and O. Pfister, “Experimental realization of multipartite entanglement of 60 modes of a quantum optical frequency comb,” *Physical review letters*, vol. 112, no. 12, p. 120505, 2014.
 - [20] S. Yokoyama, R. Ukai, S. C. Armstrong, C. Sornphiphatphong, T. Kaji, S. Suzuki, J.-i. Yoshikawa, H. Yonezawa, N. C. Menicucci, and A. Furusawa, “Ultra-large-scale continuous-variable cluster states multiplexed in the time domain,” *Nature Photonics*, vol. 7, no. 12, p. 982, 2013.
 - [21] Y. Cai, J. Roslund, G. Ferrini, F. Arzani, X. Xu, C. Fabre, and N. Treps, “Multimode entanglement in reconfigurable graph states using optical frequency combs,” *Nature communications*, vol. 8, no. 1, pp. 1–9, 2017.
 - [22] J. Nokkala, F. Arzani, F. Galve, R. Zambrini, S. Maniscalco, J. Piilo, N. Treps, and V. Parigi, “Reconfigurable optical implementation of quantum complex networks,” *New Journal of Physics*, vol. 20, no. 5, p. 053024, 2018.
 - [23] H. Yonezawa, T. Aoki, and A. Furusawa, “Demonstration of a quantum teleportation network for continuous variables,” *Nature*, vol. 431, no. 7007, pp. 430–433, 2004.
 - [24] C. Fabre and N. Treps, “Modes and states in quantum optics,” *Reviews of Modern Physics*, vol. 92, no. 3, p. 035005, 2020.
 - [25] V. Roman-Rodriguez, B. Brecht, K. Srinivasan, C. Silberhorn, N. Treps, E. Diamanti, and V. Parigi, “Continuous variable multimode quantum states via symmetric group velocity matching,” *New Journal of Physics*, vol. 23, no. 4, p. 043012, 2021.
 - [26] A. Christ, C. Lupo, M. Reichelt, T. Meier, and C. Silberhorn, “Theory of filtered type-II parametric down-conversion in the continuous-variable domain: Quantifying the impacts of filtering,” *Physical Review A*, vol. 90, no. 2, p. 023823, 2014.
 - [27] F. Arzani, C. Fabre, and N. Treps, “Versatile engineering of multimode squeezed states by optimizing the pump spectral profile in spontaneous parametric down-conversion,” *Physical Review A*, vol. 97, no. 3, p. 033808, 2018.

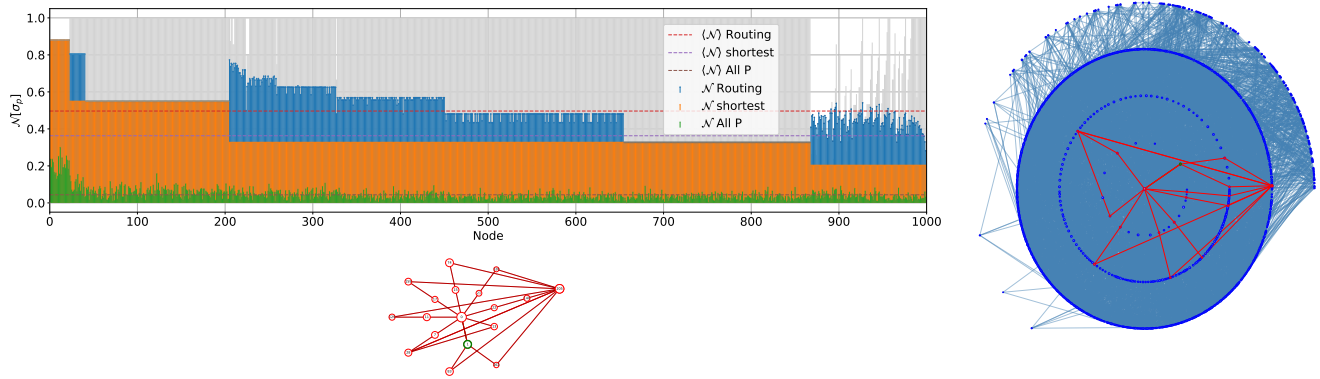


FIG. 16: Negativity produced by the three different protocols applied to each node of the $\mathcal{G}_{ER}(N = 1000, p = 0.4)$ network.

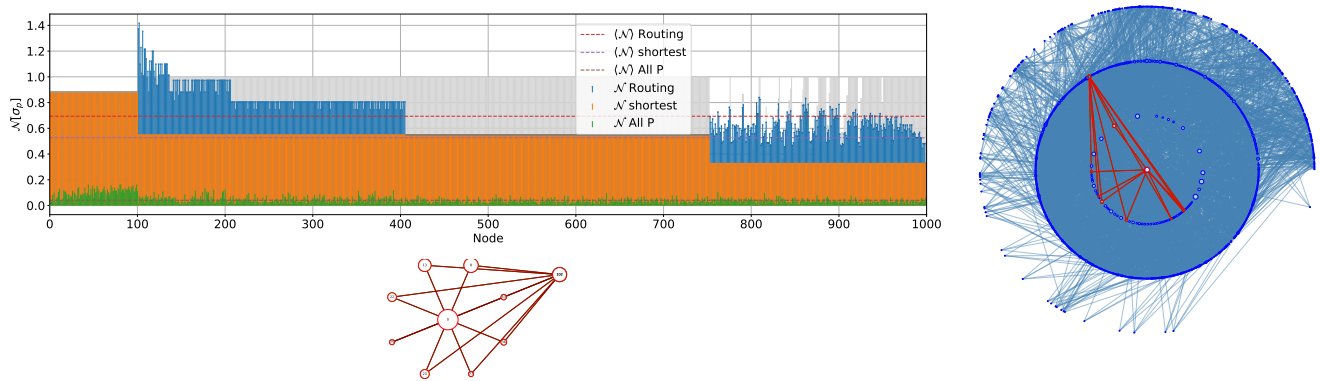


FIG. 17: Negativity produced by the three different protocols applied to each node of the $\mathcal{G}_{BA}(N = 1000, K = 4)$ network.

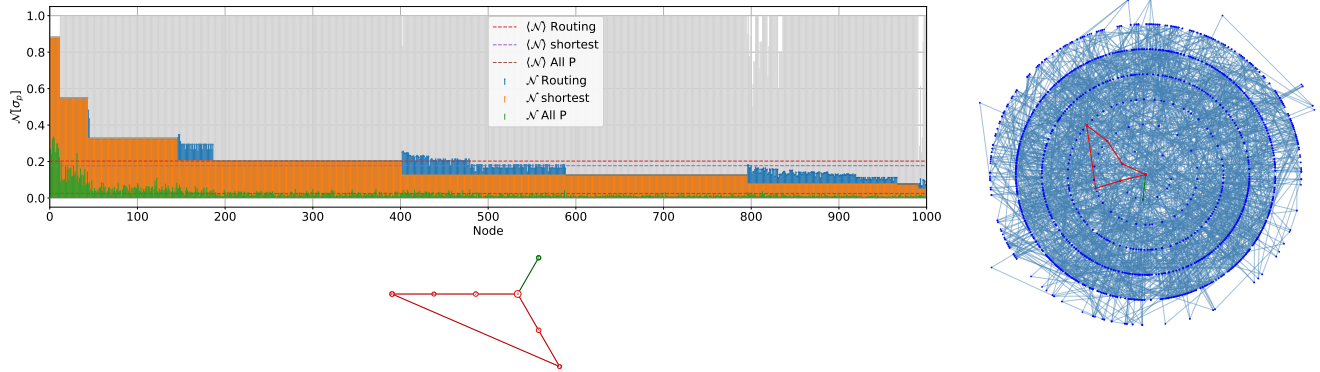


FIG. 18: Negativity produced by the three different protocols applied to each node of the $\mathcal{G}_{WS}(N = 1000, Q = 4, \beta = 0.9)$ network.

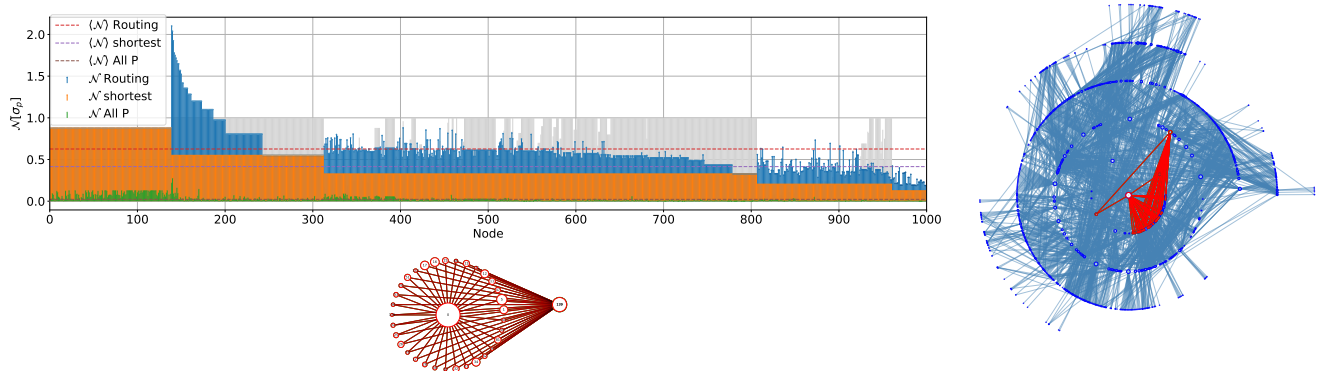


FIG. 19: Negativity produced by the three different protocols applied to each node of the $\mathcal{G}_{PP}(N = 1000, \sigma = 0.4)$ network.

- 2018.
- [28] E. Gouzien, S. Tanzilli, V. d'Auria, and G. Patera, "Morphing supermodes: A full characterization for enabling multimode quantum optics," *Physical Review Letters*, vol. 125, no. 10, p. 103601, 2020.
 - [29] M. Yukawa, R. Ukai, P. Van Loock, and A. Furusawa, "Experimental generation of four-mode continuous-variable cluster states," *Physical Review A*, vol. 78, no. 1, p. 012301, 2008.
 - [30] D. Barral, M. Walschaers, K. Bencheikh, V. Parigi, J. A. Levenson, N. Treps, and N. Belabas, "Versatile photonic entanglement synthesizer in the spatial domain," *Physical Review Applied*, vol. 14, no. 4, p. 044025, 2020.
 - [31] J. Arrazola, V. Bergholm, K. Brádler, T. Bromley, M. Collins, I. Dhand, A. Fumagalli, T. Gerrits, A. Goussev, L. Helt, *et al.*, "Quantum circuits with many photons on a programmable nanophotonic chip," *Nature*, vol. 591, no. 7848, pp. 54–60, 2021.
 - [32] N. C. Menicucci, P. van Loock, M. Gu, C. Weedbrook, T. C. Ralph, and M. A. Nielsen, "Universal quantum computation with continuous-variable cluster states," *Phys. Rev. Lett.*, vol. 97, p. 110501, Sep 2006.
 - [33] N. C. Menicucci, S. T. Flammia, and P. van Loock, "Graphical calculus for gaussian pure states," *Physical Review A*, vol. 83, no. 4, p. 042335, 2011.
 - [34] M. Gu, C. Weedbrook, N. C. Menicucci, T. C. Ralph, and P. van Loock, "Quantum computing with continuous-variable clusters," *Physical Review A*, vol. 79, no. 6, p. 062318, 2009.
 - [35] M. Walschaers, N. Treps, S. Bhuvanesh, L. D. Carr, and V. Parigi, "Emergent complex quantum networks in continuous-variables non-Gaussian states ." arXiv:2012.15608.
 - [36] F. Arzani, G. Ferrini, F. Grosshans, and D. Markham, "Random coding for sharing bosonic quantum secrets," *Phys. Rev. A*, vol. 100, p. 022303, Aug 2019.
 - [37] O. Pinel, J. Fadel, D. Braun, P. Jian, N. Treps, and C. Fabre, "Ultimate sensitivity of precision measurements with intense gaussian quantum light: A multimodal approach," *Phys. Rev. A*, vol. 85, p. 010101, Jan 2012.
 - [38] M. Gessner, L. Pezzè, and A. Smerzi, "Sensitivity bounds for multiparameter quantum metrology," *Phys. Rev. Lett.*, vol. 121, p. 130503, Sep 2018.
 - [39] L. Lami, B. Regula, X. Wang, R. Nichols, A. Winter, and G. Adesso, "Gaussian quantum resource theories," *Physical Review A*, vol. 98, no. 2, p. 022335, 2018.
 - [40] M. Idel, D. Lercher, and M. M. Wolf, "An operational measure for squeezing," *Journal of Physics A: Mathematical and Theoretical*, vol. 49, no. 44, p. 445304, 2016.
 - [41] D. Cvetkovic, M. Doob, and H. Sachs, *Spectra of Graphs: Theory and Applications*. Wiley, 1999.
 - [42] A. E. Brouwer and W. H. Haemers, *Spectra of graphs*. Springer Science & Business Media, 2011.
 - [43] M. E. J. Newman, *Networks, second edition*. Oxford University Press, 2018.
 - [44] A. L. Barabási, *Networks science*. Cambridge University Press, 2016.
 - [45] P. Erdos, A. Rényi, *et al.*, "On the evolution of random graphs," *Publ. Math. Inst. Hung. Acad. Sci.*, vol. 5, no. 1, pp. 17–60, 1960.
 - [46] M. E. Newman, "The structure and function of complex networks," *SIAM review*, vol. 45, no. 2, pp. 167–256, 2003.
 - [47] D. J. Watts and S. H. Strogatz, "Collective dynamics of 'small-world' networks," *nature*, vol. 393, no. 6684, pp. 440–442, 1998.
 - [48] R. Albert and A.-L. Barabási, "Statistical mechanics of complex networks," *Reviews of modern physics*, vol. 74, no. 1, p. 47, 2002.
 - [49] A. Elmokashfi, A. Kvalbein, and C. Dovrolis, "On the scalability of BGP: the roles of topology growth and update rate-limiting," in *Proceedings of the 2008 ACM CoNEXT Conference*, pp. 1–12, 2008.
 - [50] I. Ispolatov, P. L. Krapivsky, and A. Yuryev, "Duplication-divergence model of protein interaction network," *Physical review E*, vol. 71, no. 6, p. 061911, 2005.
 - [51] F. Mascherpa, A. Smirne, A. D. Somoza, P. Fernández-Acebal, S. Donadi, D. Tamascelli, S. F. Huelga, and M. B. Plenio, "Optimized auxiliary oscillators for the simulation of general open quantum systems," *Phys. Rev. A*, vol. 101, p. 052108, May 2020.
 - [52] I. J. Farkas, I. Derényi, A.-L. Barabási, and T. Vicsek, "Spectra of "real-world" graphs: Beyond the semicircle law," *Physical Review E*, vol. 64, no. 2, p. 026704, 2001.
 - [53] E. P. Wigner, "On the distribution of the roots of certain symmetric matrices," *Annals of Mathematics*, pp. 325–327, 1958.
 - [54] P. van Loock and S. L. Braunstein, "Multipartite entanglement for continuous variables: a quantum teleportation network," *Physical Review Letters*, vol. 84, no. 15, p. 3482, 2000.
 - [55] S. Pirandola and S. Mancini, "Quantum teleportation with continuous variables: A survey," *Laser Physics*, vol. 16, no. 10, pp. 1418–1438, 2006.
 - [56] R. Simon, "Peres-horodecki separability criterion for continuous variable systems," *Physical Review Letters*, vol. 84, no. 12, p. 2726, 2000.
 - [57] C. Weedbrook, S. Pirandola, R. García-Patrón, N. J. Cerf, T. C. Ralph, J. H. Shapiro, and S. Lloyd, "Gaussian quantum information," *Rev. Mod. Phys.*, vol. 84, pp. 621–669, May 2012.
 - [58] M. Ohliger, K. Kieling, and J. Eisert, "Limitations of quantum computing with gaussian cluster states," *Phys. Rev. A*, vol. 82, p. 042336, Oct 2010.
 - [59] M. Van den Nest, A. Miyake, W. Dür, and H. J. Briegel, "Universal resources for measurement-based quantum computation," *Phys. Rev. Lett.*, vol. 97, p. 150504, Oct 2006.
 - [60] S. K. Joshi, D. Aktas, S. Wengerowsky, M. Lončarić, S. P. Neumann, B. Liu, T. Scheidl, G. C. Lorenzo, Ž. Samec, L. Kling, *et al.*, "A trusted node-free eight-user metropolitan quantum communication network," *Science advances*, vol. 6, no. 36, p. eaba0959, 2020.
 - [61] F. Centrone, "Routing in CV-networks." *Software Heritage* repository [swh:1:dir:49a931dca9247cabcbf58a9873fa5eea6db3ce47](https://nvd.nist.gov/vuln/data-feeds#CVNVD-2021-0001) containing the numerical tools developed for this article, 2021.
 - [62] N. Acosta-Mendoza, A. Gago-Alonso, and J. E. Medina-Pagola, "Frequent approximate subgraphs as features for graph-based image classification," *Knowledge-Based Systems*, vol. 27, pp. 381–392, 2012.
 - [63] O. Jones, "Spectra of simple graphs," *Whitman College, Walla-Walla*, 2013.

Appendix A: Squeezing spectra of regular graphs

Given any graph's spectrum we can employ equation (12) to compute the amount of squeezing in each mode required to build the Gaussian network. In the following calculations we used the spectra of regular graphs known in literature. A detailed reference on the spectra of regular graphs and how to obtain them can be found here [42, 63].

We use the linear graph as a benchmark to see how the squeezing cost scales with the number of nodes and links.

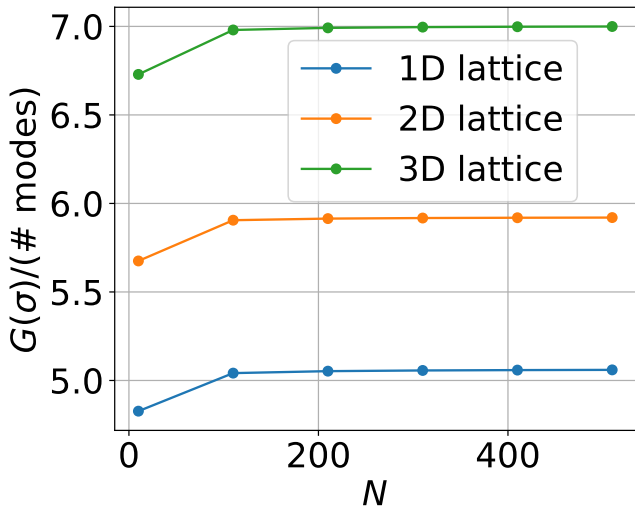


FIG. 20: Trend of the average squeezing cost per mode $\bar{G}(\sigma)$ for 1D, 2D and 3D lattices, with N , N^2 and N^3 nodes respectively. Notice that the cost becomes asymptotically constant, as predicted by the theory.

In fact, single mode squeezing and the CZ-gate both require a fixed amount of squeezing to be implemented, so we would expect $G(\sigma)$ to scale linearly with the number of links and nodes. This is a direct consequence of the spectral distribution of the linear graph, which is

$$D_k(\mathcal{L}_N) = 2 \cos \frac{\pi k}{N+1}, \quad \{k = 1, \dots, N\}. \quad (\text{A1})$$

We can use equations (12) and (18) to compute the squeezing cost exactly for any given N . For $N \gg 1$, the average squeezing cost per mode $\bar{G} = G/(\text{\#squeezed modes}) = G/\text{rk}(A)$ can be approximated by the following integral

$$\bar{G} \sim 10 \int_0^N \log_{10} \left(1 + \frac{\cos \pi y^2}{2} + \sqrt{\cos \pi y^2 + \frac{\cos \pi y^4}{4}} \right) dy \quad (\text{A2})$$

Since the integrand can be upper bounded by a constant, \bar{G} is approximately constant with N for a large number of nodes. This can be easily generalized to the case of a D -dimensional cubic lattice $\mathcal{L}_N^{(D)}$, considering that adding a new dimension would just add a new set of eigenvalues of the form (A1), as shown in section 2.6 of [41]. As a consequence, the squeezing cost of the $\mathcal{L}_N^{(D)}$ is $G = O(N^D)$, whereas the average cost per mode would be again constant with the number of nodes N , as shown in Fig. 20.

Similarly, we can use the eigenvalues expression of the circular graph (or its generalization with $Q > 1$ nearest neighbors)

$$D_k(\mathcal{G}_{C(Q)}) = \frac{\sin[(Q+1)k\pi/N]}{\sin[k\pi/N]} - 1, \quad k = \{0, \dots, N-1\}. \quad (\text{A3})$$

From this we can see why the linear and circular graph have the same scaling. In fact for $Q = 1$, we have $D_k(\mathcal{G}_{C(1)}) = 2 \cos(k\pi/N) - 1$.

The spectra of the star and diamond graph have only two non-null eigenvalues [63]

$$\{D_k(\mathcal{S}_N)\} = \{\sqrt{N-1}, 0^{N-2}, -\sqrt{N-1}\}, \quad (\text{A4})$$

$$\{D_k(\mathcal{D}_N)\} = \{\sqrt{2N}, 0^{N-2}, -\sqrt{2N}\}. \quad (\text{A5})$$

As a consequence, the cost of the star and diamond Gaussian networks grows logarithmically with N and in both cases has a simple expression

$$G(\sigma_{\mathcal{S}_N}) = 20 \log_{10} \left(\frac{1}{2}(1 + N + \sqrt{(N-1)(N+3)}) \right) \quad (\text{A6})$$

$$= 20 \log_{10} N + O\left(\frac{1}{N}\right), \quad (\text{A7})$$

$$G(\sigma_{\mathcal{D}_N}) = 20 \log_{10} \left((1 + N + \sqrt{N(N+2)}) \right) \quad (\text{A8})$$

$$= 20 \log_{10} N + 20 \log_{10} 2 + O\left(\frac{1}{N}\right), \quad (\text{A9})$$

$$(\text{A10})$$

Finally, the spectrum of the fully connected graph is

$$\{D_k(\mathcal{S}_N)\} = \{N-1, -1^{\otimes(N-1)}\}, \quad (\text{A11})$$

yielding a squeezing cost that can be expressed as two contributions

$$G(\sigma_{\mathcal{F}_N}) = 10 \left[(N-1) \log_{10} \frac{3+\sqrt{5}}{2} + \log_{10} \left(1 + \frac{(N-1)^2}{2} + \sqrt{(N-1)^2 + \frac{(N-1)^4}{4}} \right) \right] \quad (\text{A12})$$

$$= 10(N-1) \log_{10} \frac{3+\sqrt{5}}{2} + 20 \log_{10} N + O\left(\frac{1}{N}\right), \quad (\text{A13})$$

which sum up to a cost growing essentially linearly in N .

Appendix B: Graphical Calculus

In ref. [33] it is provided a unified graphical calculus for all Gaussian pure states that is particularly suited for describing highly multimode Gaussian networks.

In this framework, a N mode Gaussian state is completely described, up to displacements, by a $N \times N$ complex valued adjacency matrix:

$$Z = V + iU \quad (\text{B1})$$

Where the real and imaginary part of Z , V and U respectively, are related to the covariance matrix through the following unique decomposition

$$\sigma = \frac{1}{2} \begin{pmatrix} U^{-1} & U^{-1}V \\ VU^{-1} & U + VU^{-1}V \end{pmatrix} \quad (\text{B2})$$

Gaussian graph states have a particular simple graphical representation, being

$$Z = A + iD \quad (\text{B3})$$

Where A is the weighted adjacency matrix of the graph and D is a diagonal matrix that represents momentum squeezing, i.e. for $D = 10^{-2s} \mathbb{1}$ the momentum variance of all modes is reduced by $2s$ decibels.

All symplectic operations can be reproduced in this language, however, since we already know how to represent the resource graph states, we only need to implement the quadrature measurements in \hat{x} and \hat{p} . We can express the state as

$$Z = \begin{pmatrix} t & R^T \\ R & W \end{pmatrix} \quad (\text{B4})$$

Where t is the target mode we want to measure, W is the subgraph of the untouched modes and R their correlations with the target mode. We have the following two rules:

- $Z \longrightarrow Z_q = W$ after a \hat{q} measurement.
- $Z \longrightarrow Z_p = W - \frac{RR^T}{t}$ after a \hat{p} measurement.

Thus, for a measurement in \hat{q} we remove the node and its link from the graph, whereas for a measurement in \hat{p} we apply a $\pi/2$ phase rotation and then measure \hat{q} .

Appendix C: Parallel enhancement of entanglement

We can use the rules described in the previous sections to prove eq. (28), that expresses analytically the power of parallel enhancement of entanglement in the diamond network when measuring the central nodes in \hat{p} . Let us assume that the nodes A and B are squeezed by a factor S_A and S_B respectively, there are N central nodes and the k th mode has squeezing S_k and is correlated with A and B through a CZ-gate with strength g_{Ak} and g_{Bk} . It

can then be easily showed that the final pair will have a purely imaginary adjacency matrix of the form

$$Z_{AB} = i \begin{pmatrix} \Sigma_A & \Gamma \\ \Gamma & \Sigma_B \end{pmatrix} \quad (\text{C1})$$

Where $\Sigma_A = S_A + \sum_k \frac{g_{Ak}^2}{S_k}$, $\Sigma_B = S_B + \sum_k \frac{g_{Bk}^2}{S_k}$ and $\Gamma = \sum_k \frac{g_{Ak}g_{Bk}}{S_k}$. These result can be derived by direct application of the rule for measuring \hat{p} in the graphical calculus formalism, schematized in figure 21.

Employing eq. (B1) and (B2) and noticing that $V = 0$, we can reconstruct the covariance matrix of the final pair:

$$\sigma_f = \begin{pmatrix} \frac{\Sigma_B}{\Sigma_A \Sigma_B - \Gamma^2} & -\frac{\Gamma}{\Sigma_A \Sigma_B - \Gamma^2} & 0 & 0 \\ -\frac{\Gamma}{\Sigma_A \Sigma_B - \Gamma^2} & \frac{\Sigma_A}{\Sigma_A \Sigma_B - \Gamma^2} & 0 & 0 \\ 0 & 0 & \Sigma_A & \Gamma \\ 0 & 0 & \Gamma & \Sigma_B \end{pmatrix} \quad (\text{C2})$$

Notice that this state differs from a graph state up to a local phase.

By computing the serialian Δ of the partially transpose covariance matrix of the pair $\tilde{\sigma}_f$ and applying formula (27), we can derive the general lowest symplectic eigenvalue of the state

$$\nu_-^2 = \frac{(\sqrt{\Sigma_A \Sigma_B} - \Gamma)^2}{\Sigma_A \Sigma_B - \Gamma^2} \quad (\text{C3})$$

Finally, if we assume that all the modes are equally squeezed in \hat{p} of a factor $R^{-1} = 10^{2s}$ and all the CZ-gate correlations have a strength g , we arrive to formula (28).

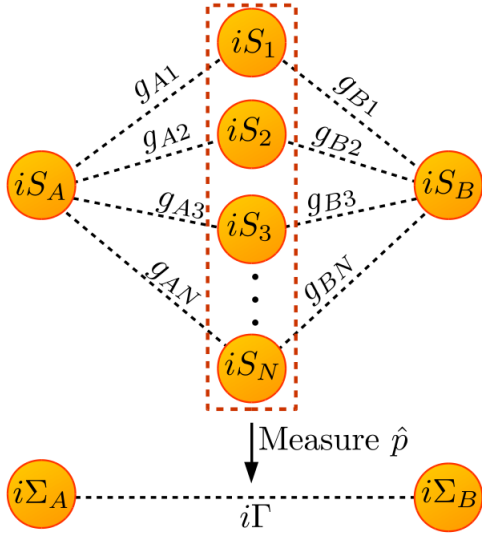


FIG. 21: Graphical representation of the diamond graph and its parallel enhancement of entanglement.